POLITECNICO DI TORINO
Repository ISTITUZIONALE

Holistic performance assessment of gridshells: Methodological framework and applications to steel gridshells

(Article begins on next page)

18 May 2024

Full length article

Holistic performance assessment of gridshells: Methodological framework and applications to steel gridshells

Lorenzo Raffaele [a],*, Luca Bruno [a], Francesco Laccone [b], Fiammetta Venuti [a], Valentina Tomei [c]

[a] *Politecnico di Torino, Viale Mattioli 39, Torino, 10126, Italy*
[b] *Institute of Information Science and Technologies (ISTI), National Research Council of Italy (CNR), Via Giuseppe Moruzzi 1, Pisa, 56124, Italy*
[c] *Università degli studi di Cassino e del Lazio Meridionale, via G. Di Biasio 43, Cassino, 00143, Italy*

ARTICLE INFO

ABSTRACT

Gridshells are a paradigmatic example of the intricate concept and analysis of building structures. Their design should simultaneously take into account different goals and meet final performances, by referring to multiple disciplinary competences such as the ones of architects, engineers, builders, and experts in mathematics and computer graphics. The present study provides a deep insight into a new framework for the holistic performance assessment of gridshells. The overall performance is quantitatively expressed as the linear combination of three partial metrics, referring to structural response, buildability and sustainability. Each partial metric combines multiple goal metrics, some defined in the current state of the art, others proposed by the Authors. The proposed method is tested with reference to three gridshells with their spring line partially unconstrained, and to their fully-constrained counterparts. This application is intended to shed light on the scarcely investigated mechanical behaviour of free-edge gridshells, and to be inspirational for future proposals of design/optimization solutions within the newborn FreeGrid international benchmark.

1. Introduction

Gridshells are lightweight form-resistant structures given by the discretization of a continuous doubly curved surface into a grid of line-like structural members. The first pioneering applications of this concept date back to 1890 and are due to Vladimir Shukhov [1], even though the term *grid shell* was introduced in the Sixties at the Institute for Lightweight Structures in Stuttgart [2]. During the second half of the 20th century, the gridshell structural type developed through the work of master designers, such as Buckminster Fuller [3], Frei Otto [4], Schlaich Bergermann und Partner [5,6]. Nowadays, a significant number of fascinating gridshell structures are widespread all over the world, covering a wide variety of forms, materials (e.g., timber [7], steel [5], bamboo [8], composite [9]) and construction types (e.g. single or double layer, bending-active or pre-formed).

Gridshell design can be quite an intricate process due to the significant number of variables affecting the performance of the built structure. The design and optimization of gridshells is naturally turned into a multidisciplinary activity jointly carried out by experts in mathematics, computer graphics, mechanics, structural engineering and architecture. Schematically, three design issues are particularly significant when dealing with gridshells.

Nomenclature

A	Generatrix arc length
b	Edge length
B	Generatrix span length
BP	Bulk Performance
C	Member cross-section
CP	Concentrated Plasticity
$\mathcal{D}$	Field of nodal displacements
d	Nodal displacement
$d_\perp$	Normal component of the nodal displacement
$d_\parallel$	Tangential component of the nodal displacement
d_j	Distance between the jth vertex and the best fitting plane π
d_p	Distance of the plastic hinge from the FE node
DG	Design Goal
DP	Distributed Plasticity
E	Young's Modulus
f	Gridshell rise/index for fth 2D entity (face, panel)
f_y	Yield stress/steel grade
F	Total number of 2D entities (face, panel)
FEM	Finite Element Method
g	Self-weight per unit length
GM	Goal Metric
GM_0	Baseline solution Goal Metric
GMNA	Geometrically and Materially Non-linear Analysis
h	Gridshell maximum height
i	Index for ith 1D entity (edge/arc/line, member, element)
j	Index for jth 0D entity (vertex, joint, node)
J	Joint type
K	Total number of Load Conditions
$\mathcal{K}$	Tangent stiffness
$\mathcal{K}_e$	Elasto-plastic stiffness
$\mathcal{K}_g$	Geometric stiffness
$\mathbf{K}^e$	Tangent stiffness matrix of the finite element
$\mathcal{K}_l$	Stiffness limit value
l_p	Length of the plastic hinge
$\tilde{l}$	Coefficient of variation of member lengths
L	Length of the spring line
L^*	Length of the free edge
LC	Load Condition
LF	Load Factor
LF_I	Load Factor inducing gridshell instability
LF_P	Load Factor inducing full plasticization of a cross section
$\widehat{LF}$	Critical Load Factor
M	Total number of 1D entities (edge/arc/line, member, element)
n_f	Number of incident vertices
N	Total number of 0D entities (vertex, joint, node)
$\tilde{N}$	Ratio of the member axial force over the critical buckling axial force

Structural mechanics issues. Gridshells are typical spatial, statically indeterminate, highly efficient structures designed to carry loads mainly – but not necessarily uniquely – through internal membrane forces. Consequently, they are exposed to elasto-plastic instability at member, local and global scale that usually govern their ultimate behaviour. A recent mapping study concerning research on gridshells has highlighted that buckling is among the five most recurrent keywords from all mapped publications [10]. A considerable number of scientific studies has investigated the influence on the stability of gridshells of several factors, such as the Gaussian

N_b^e	Critical buckling axial force
N^e	Axial force of the structural member
p_f	Face perimeter
P	Bulk performance metric
PP	Partial Performance
P_b	Buildability performance metric
P_s	Structural performance metric
P_{su}	Sustainability performance metric
q	Load per unit area
Q	Field of applied load
Q	Point load
s	Projection on the horizontal plane of the tributary area of a structural joint
S	Horizontal projection of the gridshell surface
$\check{S}$	Gridshell surface
SLS	Serviceability Limit State
ULS	Ultimate Limit State
v	Valence of 0D entities (vertex, joint, node)
W	Gridshell equivalent weight
W^*	Surface density of the equivalent weight
x, y, z	Reference axes
α	Environmental impact correction coefficient
δ_z	Maximum vertical displacement at the generic LF
$\hat{\delta}_z$	Maximum vertical displacement at SLS
$\hat{\delta}_{z,l}$	Upper limit of the vertical displacement at SLS
$\bar{\Delta}$	Face out-of-planarity metric
Δd	Increment of member displacement
Δ_f	f th face out-of-planarity metric
ΔU	Increment of the strain energy
ε_{max}	Strain ratio for initial plasticization of the cross section
ε_{min}	Strain ratio for full plasticization of the cross section
ε_y	Yield strain
ϕ	Cross-section diameter
$\gamma_s, \gamma_b, \gamma_{su}$	Weighting factors of partial performance metrics
ρ	Material density
v	Poisson's ratio
σ	Stress
$\#(C^*)$	Cardinality of the ensemble of member cross-sections scaled to the number of structural members
$\#(J^*)$	Cardinality of the ensemble of joint types scaled to the number of joints
$\#(N^*)$	Surface density of the joints

curvature of the underlying surface (e.g., [11–13]), the grid topology and spacing (e.g., [14–16]), the geometrical and mechanical imperfections (e.g., [12,17–22]), the kind of joints (e.g., [18,23–25]) and the boundary conditions (e.g., [11,13,26]). Additionally, gridshells are structures with a relatively high strength-to-weight ratio, and their serviceability may be consequently reduced by large displacements under free, live loads. To the Authors' best knowledge, such a design issue is not systematically addressed by studies in literature.

Construction issues. Gridshells are generally doubly curved structures, particularly suitable for developing free-form architecture. This peculiarity, one of the most attractive features of this structural type, involves increasing costs related to manufacturing, e.g., due to the need to fabricate non-standard elements or cover the structural grid with cladding. The following construction issues, which are strictly related to geometry, are relevant in gridshell design since they strongly impact on the construction costs.

- Connections between members: in a free-form gridshell each connection can be unique, making the costs of joint manufacturing dramatically high. The necessity to standardize connections has been successfully tackled with elastic gridshells, which are initially laid flat and can adopt a single connection detail [27,28]. The same does not hold for pre-formed gridshells, such as steel gridshells, made of straight beams connected at joints. The repeatability of joints can be improved by reducing the number of joint clusters [29]. However, uneven joints can alter the development of efficient load paths, leading to over-stressed

areas and load eccentricities. These issues can be mitigated by geometric optimization, i.e., by designing torsion-free nodes and edge-offset meshes [30].

- Planarity of faces: since gridshells are usually employed as building envelopes and separations, a major constraint is the need to be covered or infilled with panels. A good strategy for a gridshell is to adopt a mesh with planar faces so that they can be covered by flat panels, which are significantly less expensive than curved ones. While the face planarity is an inherent property of a triangular mesh, specific discretizations [31] or optimization algorithms [32–35] have to be considered in all other cases involving quad or polygonal faces. Conversely, where curved panels cannot be avoided, clustering the panels by similarity in shape and curvature can reduce the cost, allowing the reusing of the number of moulds [36–38].
- Member length: different member lengths have a minor impact on fabrication costs with respect to connections. However, uniform member length may lead to more regular panels with minimization of material loss through cutting [39,40].
- Connections between structural members and panels: in doubly curved surfaces built with straight beams, there is usually a kink angle between cladding panels and structural members [30]. The design of the beam-panel connections could be quite complex since it involves the angles between a couple of adjacent faces and the volume occupied by the elements in 3D. Small or constant kinks reduce the spacers and support size.

Sustainability issues. In recent years, great attention has been paid to sustainable design, being the carbon footprint of the construction sector approximately a third of global man-made emissions [41,42]. One of the advantages of gridshells, with respect to traditional frame systems and continuous shells, is that they are suitable for creating sustainable design since they are characterized by lower embodied energy and reduced operating energy [43]. If compared with other conventional structures (e.g. frames, spatial trusses etc.), gridshells are highly efficient employing low structural material in relation to the load they can withstand. In a circular-economy perspective, recent works demonstrate they can be also built with non-conventional or recycled materials, such as cardboard [44] or skis [45], characterized by an even lower embodied energy. However, sustainability in steel gridshell is deeply linked to the amount and type of elements and connection technology (i.e. welding, bolting, additive manufacturing etc.).

Even if the structural, construction and sustainability issues above are outlined and discussed separately for the sake of clarity, they are always connected, often negatively correlated, so that an improvement obtained for a single design aspect may worsen another. Thus, gridshell design and optimization shall be pursued by jointly taking into account all the above issues in order to increase the overall performance. In spite of this, gridshells are usually designed and optimized by separately referring to a specific performance. Even recently, a huge number of studies focus on structural performances only, e.g. [46–50]. Others studies are specifically addressed to simplify the gridshell geometry, and its construction in turn, e.g. [29,33,34,51,52]. To the Authors' best knowledge, no studies specifically address the sustainability issue in proper terms, while others (e.g. [53]) are simply intended to reduce the consumption of material rather than to consider the overall environmental impact. Conversely, to the Authors' best knowledge, only two recent studies authored by the same authoritative research team have attempted to simultaneously consider both structural and fabrication issues [54,55].

In the light of the above state-of-art, the present study is intended to offer three main elements of novelty. First, a new methodological framework for holistic performance assessment of gridshells is detailed in order to make a synthesis of the three design issues discussed above. Secondly, the methodological framework is tested on three different single-layer gridshells. For each of them, the performance assessment is carried out considering two different boundary conditions: gridshells fully hinged along their spring lines, and with their spring line partially not constrained along what is called a "free-edge". Free-edge gridshells pose a challenge since free edges contribute to deeply alter their characteristic membrane mechanical behaviour. In spite of their widespread use in the design practice, free-edge gridshells have been scarcely studied in systematic terms except for a single, recent paper [26]. Thirdly, this study is carried out in the near wake of the newborn FreeGrid benchmark [56,57]. In the FreeGrid perspective and for future reference, the outcomes of the study are intended to provide to the wide scientific and technical community an in-depth, solid and shared background knowledge about the three baseline gridshells adopted in the benchmark.

The paper develops through the following Sections: in Section 2, the proposed methodological framework for holistic performance assessment is described in detail; Section 3 describes the geometrical and structural setups of the adopted case studies; results are presented and discussed in Section 4, while conclusions and perspectives are outlined in Section 5.

2. Methodological framework for performance assessment

The proposed framework for gridshell performance assessment aims at being:

  i. design-inspired and optimization-oriented, in the sense that the performances follow from related design goals;
 ii. analytic, in the sense that the overall performance is dissected in multiple quantitative metrics, one for each design goal;
iii. analytically comparative among different design solutions to the same problem or to different ones, in the sense that each metric is normalized with respect to a gridshell characteristic quantity to filter out the specific design problem;
 iv. holistic, in the sense that it combines multiple heterogeneous performance aspects proper to different fields as a whole;
  v. synthetically comparative with respect to an initially guessed gridshell solution in response to a given design problem, in the perspective of improving its relative performance.

In the following, the aims above are systematically and specifically recalled in commenting the key components of the framework.
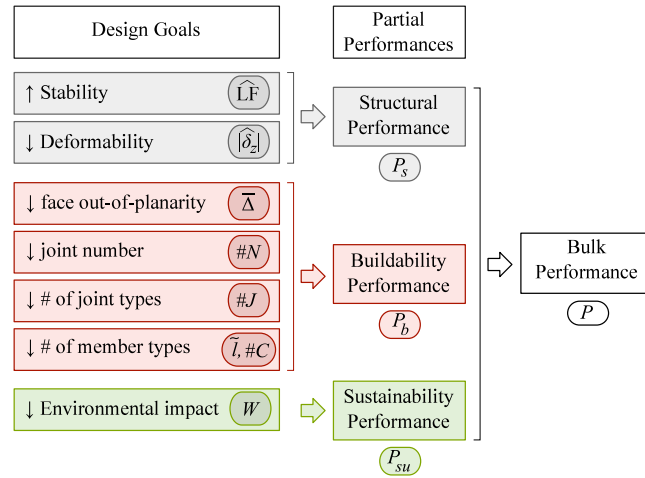
Fig. 1. Scheme of the methodological framework: from Design Goals to Partial Performances and Bulk Performance.

The proposed framework is graphically schematized in Fig. 1. For each conceptual part of the scheme, the nomenclature of the corresponding quantitative metric is given in rounded boxes. The scheme retraces the usual design workflow, i.e. from setting the goals of the design to the synthetic performance assessment of the solution. The approach moves from 7 selected Design Goals (DG, aim i.). For each of them, a quantitative Goal Metric (GM, aim ii.) to be increased or decreased is defined ($\uparrow$ and $\downarrow$ in Fig. 1, respectively). Each GM is *normalized* with respect to a relevant gridshell *characteristic quantity* (e.g. the span length, the surface area, or a mesh measure) or to a design target (e.g. a limit value of the structural response), to allow the direct comparison among multiple solutions to a single or different design problems (aim iii.). In the following, the normalized GMs are generally marked by the superscript "$*$". DG and GMs can be ascribed to 3 categories, namely *structural*, *buildability* and *sustainability* ones. GMs belonging to the same category are combined in a Partial Performance (PP) metric (aim iv.). Finally, the 3 PP metrics are combined in turn in a single Bulk Performance (BP) one to concisely quantify the overall performance of the gridshell (aim iv.). For the sake of clarity, the framework is analytically described in reversed order in the following, that is from BP to GMs nested expressions.

The BP metric P is expressed as a linear combination of the PP ones as:

$$P = \gamma_s P_s + \gamma_b P_b + \gamma_{su} P_{su}, \tag{1}$$

where P_s, P_b, P_{su} are the PP metrics related to structural response, buildability and sustainability, respectively, and γ_s, γ_b, γ_{su} are the corresponding dimensionless weighting factors constrained by $\gamma_s + \gamma_b + \gamma_{su} = 1$. These partial weighting factors allow to give different relative importance to each performance category, i.e. designers are free to adjust such values to push a gridshell towards specific design conditions. However, in what follows we set $\gamma_s = \gamma_b = \gamma_{su} = 1/3$, so to accord the same importance to each category. The adopted additive form (1) necessarily requires the PP metrics are homogeneous quantities. Conversely, structural, buildability and sustainability PP metrics and related GMs are arguably different, so that ensuring the same unit of measure for all of them is hardly viable. A *dimensionless form* of the PP or GM metrics allows fulfilling the requirement above and can be obtained by relating such values to the metrics of a *baseline solution*. In the following, these latter are marked by the subscript "0". In such a way, the PP and BP metrics express the relative performance of a solution with respect to an initial one (aim v.). In the current form of the proposed approach, we choose to make GMs dimensionless at source, and then to obtain in the same form the PP and BP metrics.

In the next three subsections, each PP metric is expressed through the corresponding GMs.

2.1. Structural performance

The setting of the structural performance obeys to the following conceptual guidelines:

- Gridshells are form-resistant structures, and traditionally the design and optimization of their shape mainly focus on their structural performances (e.g. [48,58,59]);
- Even if gridshells stability at Ultimate Limit State (ULS) has primarily attracted the attention of designers and scholars (e.g. [11,12,17]), the structural performances at Serviceability Limit State (SLS) should be also accounted for;
- The definition of the structural performance P_s and related GMs cannot be separated from the mechanical model adopted to obtain them.

In the light of the above, the mechanical model adopted in the study is briefly motivated and described first, and then the structural performance metric P_s is analytically defined.

2.1.1. Adopted mechanical model

Among the models available in scientific literature and design practice to describe the mechanical behaviour of a gridshell (e.g. Linear Elastic Analysis, Linear Buckling Analysis, Geometrically Nonlinear Analysis, Geometrically and Materially Nonlinear Analysis), GMNA is adopted in this study in the light of the main issues of this kind of structures, as previously introduced.

GMNA is able to assess the strength capacity of a structure accounting for both plasticity and buckling failure modes under large displacements. GMNA solves the nonlinear equation:

$$\left[\mathcal{K} + \mathcal{K}_e(D) + \mathcal{K}_g(D)\right] D = \text{LF} \, Q \tag{2}$$

where D is the displacement field, Q the field of applied loads, LF the load multiplier (Load Factor in the following), $\mathcal{K}$ the tangent stiffness at origin, $\mathcal{K}_e$ and $\mathcal{K}_g$ the elasto-plastic and geometrical ones, respectively, both functions of the displacement field.

The overall structural behaviour results from the tangent stiffness matrix at origin $\mathcal{K}$ which softens and/or stiffens due to progressive yielding and/or second order effects under monotonically increasing load.

It is well known that buckling instability of single-layer gridshells and their design/optimization are highly sensitive to imperfections (e.g. [21,22]). For the sake of simplicity, in the present study, GMNA is uniquely carried out on the perfect structure. Thus, the effects of any kind of imperfections induced by constraints, load conditions, mechanical properties, or geometrical features are neglected even if the proposed methodological framework has a general validity and can easily account for them. This choice is motivated by two considerations: (i) the choice of the imperfection model is still an object of debate in the civil engineering community (e.g. [12,21]); (ii) the computational testing of a gridshell allows decoupling the study of the core structural performance from its imperfection sensitivity, thus it is possible to isolate and discuss only the parameters of interest.

In order to properly follow the progressive member yielding, the Distributed Plasticity (DP) approach with nonlinear behaviour modelled along the member and over its cross section [60] is adopted as a priority, even if a Concentrated Plasticity (CP) approach [61] is also used for comparison.

The structural members are modelled using cubic two-node beam elements based on Timoshenko beam theory, with three integration points along the length, so that bending moments are exactly represented until a quadratic variation. Each structural member is discretized by 4 Finite Elements (FEs) in order to accurately simulate second-order effects along the beam length and related member instability, even if single FE discretization is discussed for comparison.

The Load Control procedure is applied within GMNA by setting a fixed load step magnitude equal to 1/1000 the magnitude of the load Q. The iterative convergence is accomplished at each step by means of the standard Newton Raphson method by setting a tolerance equal to 5e–3 in terms of weighted residuals of the variables.

GMNA is carried out on Finite Element code ANSYS® Mechanical APDL r22.2 [62,63]. The code SAP2000® v21 [64] is adopted for comparison.

2.1.2. Structural goal metrics

The proposed novel structural performance metric P_s depends on and is averaged over the K retained Load Conditions LC_k:

$$P_s = \frac{\sum_{k=1}^{K} \frac{\widehat{\text{LF}}_k}{\widehat{\text{LF}}_{k,0}} \Big/ \frac{|\hat{\delta}_{z,k}^*|}{|\hat{\delta}_{z,k,0}^*|}}{K}, \tag{3}$$

where the GM at SLS is the maximum vertical displacement over the whole gridshell $\hat{\delta}_z$, the GM at ULS is the critical Load Factor $\widehat{\text{LF}}$.

Deformability at SLS. At SLS, gridshells structural performances are driven by their deformability. The magnitude of the maximum vertical displacement over the whole gridshell $\hat{\delta}_{z,k}$ under the kth Load Condition LC_k is retained as the DG quantitative metric to be reduced. The DG metric is normalized with respect to the upper limit of deformability for gridshells $\hat{\delta}_{z,l}$, in formulas $\hat{\delta}_{z,k}^* = \hat{\delta}_{z,k}/\hat{\delta}_{z,l}$. In the technical literature, there is no general agreement about such a design target. By way of example, $\hat{\delta}_{z,l}$ is set equal to $B/200$, $B/300$, $B/400$ respectively in [65–67], being B the gridshell span. In the present study, $\hat{\delta}_{z,l} = B/200$ is conventionally set. Such a normalization not only allows to compare among them different design solutions for multiple design problems having different spans, but has also a clear design meaning: $\hat{\delta}_{z,k}^* \leq 1$ certifies a design solution meets the serviceability performance level.

Behaviour at ULS. At ULS, gridshells structural performances are affected by several modes of failure involving their stability and strength. In the present study, the critical Load Factor $\widehat{\text{LF}}$ is retained as the DG quantitative metric to be increased. It is classically defined as

$$\widehat{\text{LF}} = Q_u/Q, \tag{4}$$

where Q_u is the magnitude of the ultimate load and Q is the one of the design load defined for the generic Load Condition LC. This DG metric does not need normalization, being such by definition thanks to reference to the design load: $\widehat{\text{LF}} \geq 1$ certifies a design solution meets the ultimate performance level.

In particular, in the proposed methodological framework it rigorously accounts for global, local and member instability, and cross-section plasticization, if any. It is analytically defined as

$$\widehat{\text{LF}} = \min\left(\text{LF}_I, \text{LF}_P\right), \tag{5}$$

i.e. as the minimum load multiplier among the LF_I inducing the instability of the gridshell, and the LF_P corresponding to the full plasticization of at least a single cross section of one structural member (Fig. 2a). In the following, each load multiplier is analytically defined.
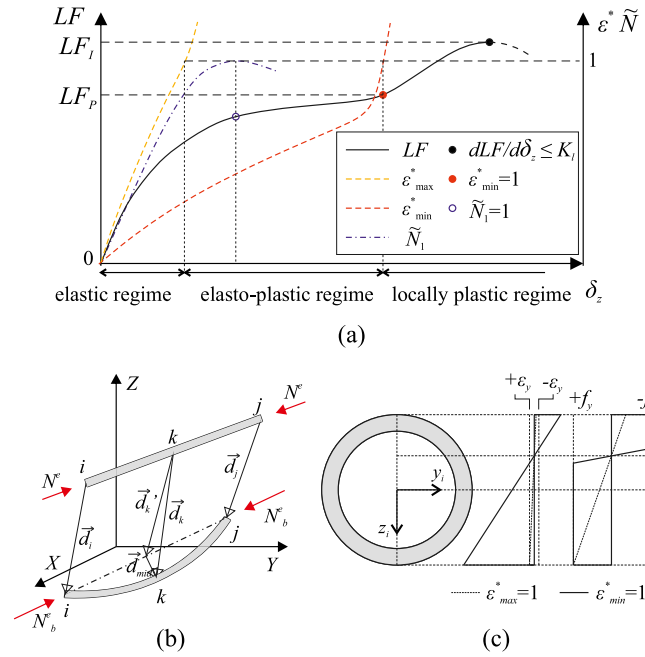
Fig. 2. Structural performance: Conceptual graphical scheme exemplifying the variables used for establishing the critical load factor $\widehat{\mathrm{LF}}$ as the minimum between LF_I and LF_P (a), the member buckling (b, after [68]), and the member cross-section yielding (c).

Gridshell instability. Gridshell instability is usually categorized according to the amount of structural joints involved in the collapse. "Global", "local" or "member" instabilities are conventionally referred to. Global instability involves the structure buckling as a whole, while local instability involves the snap-through of single or multiple adjacent joints, and member instability refers to the buckling of a single structural member [12]. In spite of this conceptual categorization, the final effects of member, local and global instabilities are hard to quantitatively distinguish: i. a generally valid watershed number of joints cannot be universally defined to discriminate local and global instability. Indeed, a continuous measure of the degree of globalness of the instability called Buckling Shape Length has been recently proposed in [21]; ii. single-member buckling, local and global instability at increasingly larger scales usually interacts in statically indeterminate gridshells [11]. Such an interaction may take place in the form of progressive instability or synchronous instability [68]. The former implies the gradual propagation of a single-member buckling to multiple members or to the snap-through of a single joint [69], up to the global collapse face to a monotonically increasing load. The latter is accompanied by the buckling of multiple members and the overall instability for nearly the same value of the load multiplier, and usually takes place in highly optimized gridshells [70].

The buckling of single members subjected to axial force and biaxial bending moments, if any, is detected by using the method initially proposed by [71]. The axial compression force N^e versus the lateral relative flexural deflection d_{mid} of the mid-point of the member is traced, as defined in Fig. 2(b). In order to provide a quantitative observable of the occurrence of member buckling, the dimensionless ratio $\tilde{N} = N^e/N_b^e$ is evaluated for each member, being N_b^e the critical buckling axial force. Buckling condition clearly takes place for $\tilde{N} = 1$. Fig. 2(a) includes both the $\tilde{N}_1$-δ_z curve and the $\tilde{N}_1 = 1$ point referred to the first buckled member, for illustrative purposes only: in fact, the latter may lie in the elastic, elasto-plastic or plastic regimes, and may be followed by further buckled members. According to [71], the member buckling condition is double checked by evaluating the increment of the strain energy defined as $\Delta U = 1/2 \Delta d^t \mathbf{K}^e \Delta d$ for each Finite Element (FE), being Δd the increment of member displacement and $\mathbf{K}^e$ the FE tangent stiffness matrix. Member buckling condition takes place for $\Delta U < 0$.

Finally, whichever is their spatial extent and the eventual previous occurrence of member buckling, gridshell instability can be detected by the singularity of the global tangent stiffness matrix. Hence, the single Load Factor LF_I is defined by referring to the load–displacement curve (see Fig. 2a) as the condition

$$\mathrm{LF}_I \mid \frac{d\mathrm{LF}}{d\delta_z} \leq \mathcal{K}_l, \tag{6}$$

where the limit value $\mathcal{K}_l$ of the stiffness is ideally null, and numerically set as $\mathcal{K}_l = 0.02\mathcal{K}$, i.e. the 2% of the stiffness at origin.

Member plasticization. Besides or jointly with instability issues, members may also be subjected to *cross-section yielding* (e.g. [12,72]), especially in the case of free-edge gridshells. The member cross-section may partially or totally plasticize depending on the distribution of cross-section internal stresses $\sigma(z)$ and strains $\varepsilon(z)$ (see Fig. 2(c)). In order to provide a quantitative observable

of the degree of plasticization of the most stressed member in the gridshell, two new indices are proposed:

$$\varepsilon_{\min}^* = \max_{i=1:M} \left[\frac{\min_z \varepsilon(z)}{\varepsilon_y} \right]_i \tag{7}$$

$$\varepsilon_{\max}^* = \max_{i=1:M} \left[\frac{\max_z \varepsilon(z)}{\varepsilon_y} \right]_i \tag{8}$$

where subscript i refers to a generic member, M is the total number of members, $\min_z \varepsilon(z)$ and $\max_z \varepsilon(z)$ stand for minimum and maximum value of the strain along the local axis z, and ε_y is the material yield strain. According to Eqs. (7)–(8), ε^* is included within $[0, +\infty)$, $\varepsilon_{\max}^* = 1$ determines the plasticization of the first fibre in the most stressed beam, i.e. the occurrence of the gridshell elasto-plastic regime, while $\varepsilon_{\min}^* = 1$ determines the full plasticization of the member cross-section, i.e. the occurrence of a plastic hinge and the onset of the gridshell plastic regime. The Load Factor LF_P inducing the onset of the first plastic hinge is defined by referring to the $\varepsilon_{\min}^*$ - $\hat{\delta}_z$ curve and the $\varepsilon_{\min}^* = 1$ point (see Fig. 2a) as the condition

$$LF_P \mid \varepsilon_{\min}^* = 1. \tag{9}$$

2.2. Buildability performance

The setting of the buildability performance obeys to the following conceptual guidelines:

- In general, gridshells may assume freeform shapes that can have low modularity. As geometric complexity plays a leading role and construction materials are usually limited in forms and shapes, novel "fabrication-aware" geometric modelling and optimization tools filter the digital design domain [55,73,74], forming the new research field called Architectural Geometry. Despite their central role, referential buildability performances are not unambiguously defined in literature because of the difficulty of encompassing all possible varieties of shapes, tessellations and construction technologies;
- For the sake of generality, the DGs and related metrics are selected to build a rigorous buildability performance model, even though intentionally not all-encompassing;
- Excluded metrics are dependent on the gridshell technology and detailing system, such as the joint connection (e.g., bolted, welded, additively manufactured), and the positioning of the panel and its supporting structure with respect to the member axes and the joints (e.g., kinks at joints, edge offset [30]);
- For computing the metrics, a mesh is used as a structured geometric data model, in which the faces are coincident with the cladding panels, the edges with line-like structural members, and the vertices with structural joints. Hence, in a truly conceptual design perspective, the selected buildability metrics refer to the ideal geometry of the mesh, i.e. without thickness.

The buildability performance metric P_B is analytically defined as the arithmetic average of 5 GMs as

$$P_b = \cfrac{1}{\cfrac{1}{5} \left[\cfrac{1+\bar{\Delta}}{1+\bar{\Delta}_0} + \cfrac{\#(N^*)}{\#(N_0^*)} + \cfrac{\#(J^*)}{\#(J_0^*)} + \cfrac{1+\bar{l}}{1+\bar{l}_0} + \cfrac{\#(C^*)}{\#(C_0^*)} \right]}. \tag{10}$$

In the following, each proposed GM is defined and discussed.

Face out-of-planarity. Face planarity is a preferred requirement for double curved gridshells, as a sufficient even if not necessary condition to adopt flat cladding panels. Practically, the cost of panelling is strictly related to its size and shape, material, construction tolerances, curved forming and fastening technology, among others. Nevertheless, all other factors held constant, flat panels are cheaper than competitors: providing curved panels involves energy-intensive processes, e.g. heating and/or pressure, or additional supporting elements, e.g. to provide restraints in cold bent panels.

In what follows, the out-of-planarity Δ_f of a single generic polygonal face is expressed in merely geometric terms as the average over the n_f incident vertices of the distance d_j between the jth vertex and the best fitting plane π, normalized by the face half perimeter p_f (Fig. 3) [75,76]:

$$\Delta_f = \frac{\frac{\sum_{j=1}^{n_f} |d_j|}{n_f}}{0.5 p_f}. \tag{11}$$

According to Eq. (11), Δ_f is included within $[0, +\infty)$, where $\Delta_f = 0$ denotes a perfectly planar face, and $\Delta_f = +\infty$ a degenerate folded face. The global metric of the out-of-planarity $\bar{\Delta}$ is defined as the average over the whole number of the gridshell faces F of the fth face out-of-planarity metric Δ_f, or in formulas:

$$\bar{\Delta} = \frac{\sum_{f=1}^{F} \Delta_f}{F} \tag{12}$$

It should be noted that $\bar{\Delta}$ is normalized by definition thanks to the local and global scaling of Δ_f with respect to p_f and F, respectively.
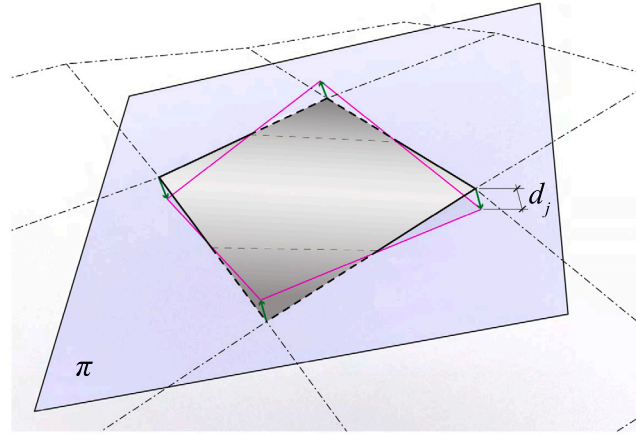
Fig. 3. Face out-of-planarity metric: the values d_j are the distances between the face vertices and their projection on the best fitting plane π. After [75].
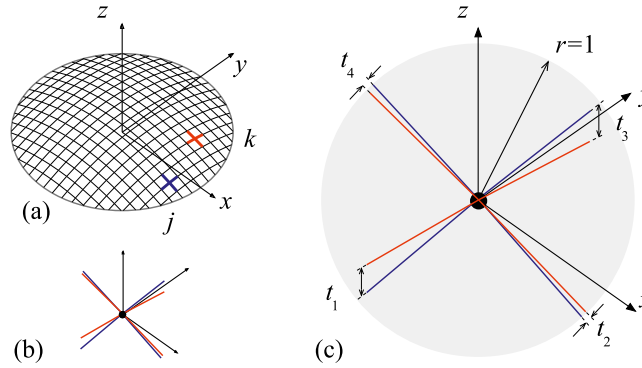

Fig. 4. Similarity metric between two vertices (in red and blue, a): the vertices are moved to the origin (b); the averaged distance of the normalized edges is evaluated (c). After [29]. (For interpretation of the references to colour in this figure legend, the reader is referred to the web version of this article.)

Joint number. The number of structural joints largely affects the overall cost and buildability. The adopted metric to be decreased is the cardinality of the ensemble of the structural joints normalized to the gridshell surface $\check{S}$, i.e. in formulas $\#(N^*) = \#(N)/\check{S}$. In other terms, $\#(N^*)$ is the surface density of the joints. $\#(N)$ is included within $[4, +\infty)$, where the lower bound $\#(N) = 4$ corresponds to the number of joints connecting three 1D structural members in the 3D space.

Uniformity of structural joints. The DG is aimed at shortening the joints chart, but also increases the visual uniformity of the gridshell topology. The adopted metric to be decreased is the cardinality $\#(J)$ of the ensemble of the joint types [29], or in geometrical terms the number of clusters of congruent vertices, normalized to the overall number of joints, i.e. in formulas $\#(J^*) = \#(J)/N$. Two vertices are congruent if they have the same valence v (the number of edges incident to a vertex) and similar shape. The shape similarity results from the closeness of the layout of the edges that are incident to the jth and kth vertices, and it is quantified by the metric S_{jk}:

$$S_{jk} = min_{|v!}\left(\sqrt{\frac{\sum_{i=1}^{v} t_i^2}{v}}\right). \tag{13}$$

S_{jk} is the minimum over all permutations among edges of the average distance between the corresponding normalized edges incident to a generic pair of vertices j and k (Fig. 4).

The number of clusters is computed according to an iterative procedure with the Farthest Point Sampling Algorithm [77], assigning a vertex in a cluster as the reference vertex (e.g. the j vertex). Then, the similarity metric is computed for the reference vertex and every other (k) vertex, verifying the condition:

$$max(S_{jk}) \leq 0.01 \tag{14}$$

If the condition is not satisfied, a new reference vertex is added. The procedure continues until the condition is verified for all vertices in the mesh. A joint belongs only to the cluster to whose reference vertex is closer, i.e., for which S_{jk} is minimum. $\#(J)$ is

included within $[2, N]$, where the lower bound $\#(J) = 2$ ideally refers to a single type for all the internal joints, plus another one used along the gridshell boundary and necessarily having different valence.

Uniformity of structural members. The DG is aimed at shortening the members chart, but also affects the visual homogeneity of the gridshell structural components. In what follows the member type results from its length and cross section. The corresponding metrics to be decreased are the coefficient of variation of member lengths $\tilde{l}$ [39], and the cardinality of the ensemble of the member cross-sections $\#(C)$ normalized to the overall number of structural members M, i.e. in formulas $\#(C^*) = \#(C)/M$. $\tilde{l} = std(l)/\bar{l}$ and $\#(C)$ are included within $[0, +\infty)$ and $[1, M]$, respectively, where the lower bounds correspond to a gridshell having all the M structural members with the same length and cross section.

The lower bounds of all the buildability GMs indicate the optimal design target in absolute terms. The normalization of Δ_f, $\#(N)$, $\#(J)$, $std(l)$ and $\#(C)$ by F, $\hat{S}$, N, $\bar{l}$ and M, respectively, allow the direct comparison of a single GM among design solutions to different design problems without necessarily referring to a baseline design solution.

2.3. Sustainability performance

The setting of the sustainability performance obeys to the following conceptual guidelines:

- weight reduction is the traditional, widespread and largely emphasized design objective for structures in general, and for lightweight ones in particular, gridshells included [53]. In such a well-established perspective, weight reduction is intended to reduce the consumption of material, e.g. usually steel in single-layer form-passive gridshells [78];
- nevertheless, the steel weight reduction alone may be a misleading criterion in a Life Cycle Assessment (LCA) perspective, as the choice of the product has become of primary importance in view of sustainable structures;
- in order to reduce the intricate analysis linked with LCA in a compact model, a single bulk weighting factor is considered to express the environmental impact of the type of the structural member cross-section and of the steel grade.

The proposed model clearly depends on the assumptions taken above. Even if the following sustainability GM may look simplistic and debatable, it has the ambition to identify a coherent trend amongst different design solutions.

As a result, the sustainability performance metric P_{su} compactly reads as

$$P_{su} = \frac{1}{W^*/W_0^*}. \tag{15}$$

where W^* is the adopted quantitative GM to be decreased, i.e. the equivalent weight proportional to the embodied carbon normalized by the gridshell surface $\check{S}$, analytically expressed as

$$W^* = \frac{W}{\check{S}} = \frac{\sum_{i=1}^{M} g_i l_i \alpha_i}{\check{S}}, \tag{16}$$

where the summation over the M structural members includes for the ith of them the material weight per unit length g_i, the length l_i, and the new "environmental impact correction coefficient" α_i. In short terms, W^* is the surface density of the equivalent weight. In the proposed framework, the embodied carbon exclusively accounts for structural members while other sources (e.g. joint manufacturing, assembly) are not considered. The proposed dimensionless environmental impact correction coefficient depends on the steel grade f_y and the category of member cross section. It is based on the "embodied carbon coefficient" for the A1–A3 phase proposed in [79] and used since some years in real LCA in order to take advantage of a producer-independent, huge, freely available database, and of a direct comparison. The technical literature proposes values for some steel grades and different products [80]; herein they are extrapolated over the range of products in order to have a homogeneous and consistent approach, and normalized with respect to hollow sections made of S355. The resulting linear fitting law of α takes the form

$$\alpha = a + 0.0002 \, f_y, \tag{17}$$

where f_y is expressed in [MPa], and a = 0.475, 0.641, 0.792, 0.939 for I/H/C/L sections, round bars and rods, plates and flats, hollow and welded sections, respectively (Fig. 5). W is included within $(0, +\infty)$, where the lower bound ideally corresponds to a gridshell without any environmental impact, i.e. a weightless gridshell or made by a zero-embodied carbon material. In other terms, analogously to the buildability GMs, the lower bound is the absolute optimal design target.

3. Description of the case studies

The methodological framework outlined in the previous section is tested on three case studies, which are the gridshells adopted by the FreeGrid benchmark (Fig. 6). Specifically, three types of single-layer gridshell geometries are considered: i. a barrel vault, with simple curvature; ii. a parabolic dome, with double Gaussian positive curvature; iii. a hyperbolic paraboloid, with double Gaussian negative curvature. For each case study, the performance assessment is discussed considering two different boundary conditions:

- the gridshells with their spring line partially not constrained along what is called a "free-edge" (referred to as "Design Baseline Gridshells" in the FreeGrid nomenclature) are retained as design baseline solutions, and their GM/PP metrics labelled by the subscript "0";
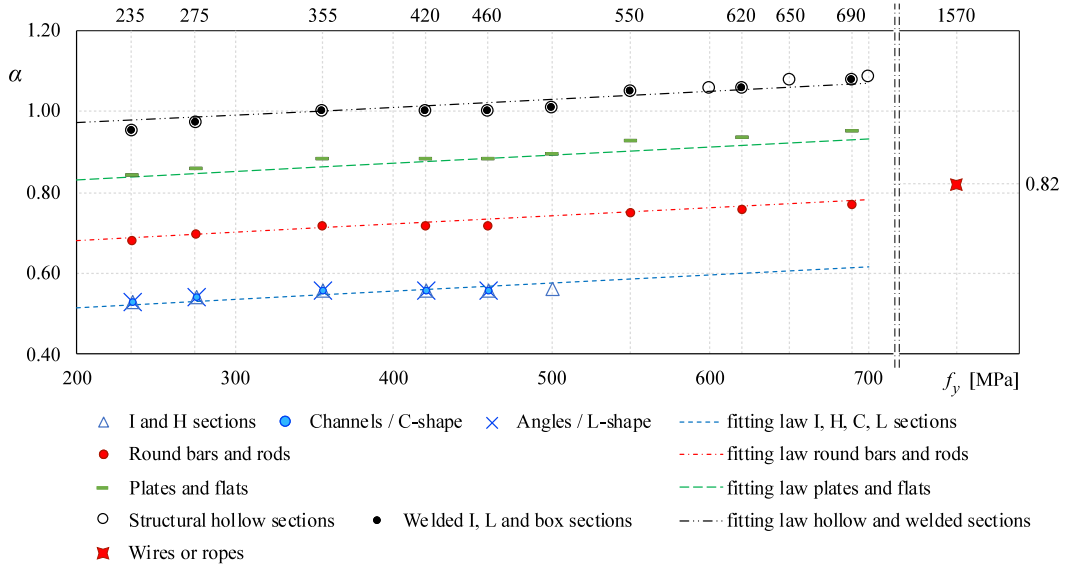
Fig. 5. Environmental impact correction coefficient α versus steel grade and type of member cross section.
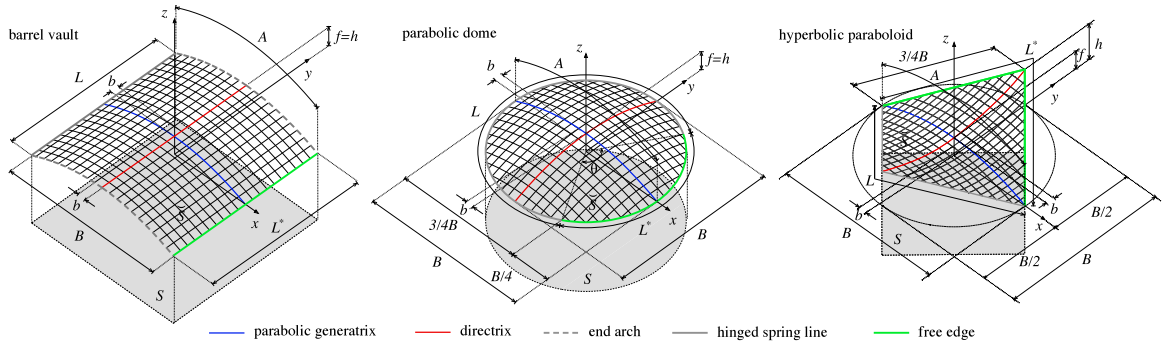

Fig. 6. Baseline design solutions: barrel vault, parabolic dome and hyperbolic paraboloid.

- the corresponding structures fully hinged along their spring lines (in the following "fully-constrained", "Background Gridshells" in the FreeGrid nomenclature) are adopted herein as dummy design solutions whose relative performances are to be evaluated with respect to the free-edge counterparts. Such design solutions exclusively differ from the free-edge gridshells for the external constraints, while all the other geometrical and structural features hold. Although such solutions may appear trivial to the designer's eye and do not fulfil the FreeGrid design constraints, they are intentionally adopted for the sake of simplicity, and in order to avoid any kind of influence on the design solutions possibly proposed by the participants to the benchmark. As a consequence of this choice, the fully-constrained gridshells are expected to perform differently from the free-edge gridshells purely from the structural perspective, thus allowing to provide a deep comparative analysis of the free-edge gridshells structural behaviour.

3.1. Geometrical setups

The main features of the gridshell geometries are illustrated in Fig. 6. All the gridshells share the same parabolic generatrix, described by the equation:

$$z = -\frac{x^2}{2B} + f, \text{ in } \left\{ -\frac{B}{2} \le x \le \frac{B}{2}, y = 0 \right\}. \tag{18}$$

For all gridshells, $B = 30$ m is the span length, $f = B/8$ the rise and its arc length A is:

$$A = B \left[\frac{\sqrt{5}}{4} + \ln\left(\frac{1+\sqrt{5}}{2} \right). \right] \approx 1.04B \tag{19}$$

Table 1
Specific geometrical features of each baseline design solution.

	Barrel vault	Parabolic dome	Hyperbolic paraboloid
Directrix equation	$z = f$	$z = -\dfrac{y^2}{2B} + f$	$z = \dfrac{y^2}{2B} + f$
h	$B/8$	$B/8$	$B/4$
L	A	$2/3\pi B$	$3/2B$
L^*	L	$L/2$	L
S	BL	$\pi B^2/4$	$B^2/2$

Table 2
Cross-section dimensions of the structural members.

	Barrel vault	Parabolic dome	Hyperbolic paraboloid
Section type	O/139.7/14.2	O/101.6/10	O/101.6/10
Area [mm^2]	5596	2876	2876
Inertia [mm^4]	11 157 936	3 052 611	3 052 611

Conversely, the three gridshells differ in their directrix, whose equations are defined in the domain $\{-B/2 \leq y \leq B/2, x = 0\}$, and summarized in Table 1 together with other characteristic dimensions (refer to Fig. 6 for nomenclature): h is the maximum height above the horizontal reference plane, i.e., the horizontal plane $z = 0$; L and L^* are the lengths of the continuous spring line and free edge, respectively; the surface extent S corresponds to the area encircled by the projection of the continuous spring line, free edge and end arches, if any, on the horizontal reference plane. Both directrix and generatrix are divided into 20 edges of constant length $b = A/20 \approx 1.56$ m. The three gridshells share the same kind of homogeneous grid made by $b \times b$ planar quadrangular square faces, except for the faces along the spring line, where the grid intersects the boundary. It follows that the running grid density is equal to $1/(b^2/2) \approx 0.82$ [1/m^2] for all gridshells, i.e. the tributary surface for all structural members is equal to 1.217 m^2, except for the irregular cells adjacent to the boundaries.

3.2. Structural setups

The structural setup is described in the following in terms of properties of the structural members, external and internal constraints, retained load conditions.

3.2.1. Structural members

The structural members of all gridshells are made of steel with a bilinear elastic-perfect plastic constitutive law. Specifically, steel S355 is adopted, with density $\rho = 7850$ kg/m^3, Young's Modulus $E = 210000$ MPa, Poisson's ratio $v = 0.3$ and yield strength $f_y = 355$ MPa. All structural members of each baseline geometry have the same section. The section dimensions together with their main inertial properties are summarized in Table 2, where "O" stands for circular hollow section, followed by its external diameter and thickness, both expressed in mm.

3.2.2. External and internal constraints

External constraints at the structural joints along the spring lines L are perfect hinges, except for the head arches of the barrel vault. The latter are allowed to move in y direction in order to avoid non-linear stiffening induced by the y-wise members. All the internal structural joints are rigid. The structural joints along the free-edge length L^* in free-edge gridshells are not constrained.

3.2.3. Load conditions

Two Load Conditions are considered and depicted in Fig. 7. They are ideal and simplified load conditions, whose moduli have been defined with the same order of magnitude of standardized design loads on gridshells.

The first symmetric Load condition LC$_1$ includes the self-weight of structural members and point loads $Q_{1,j} = q_1 s_j$ applied at all structural joints, where s_j is the projection on the horizontal reference plane of the tributary area of the jth joint. The distributed load q_1 accounts for both the weight of glass glazing and the snow load.

The second asymmetric Load condition LC$_2$ includes the self-weight of structural members and point loads $Q_{2,1,j} = q_1 s_j$ and $Q_{2,2,j} = q_2 s_j$ applied according to the following rule:

- $Q_{2,1,j}$ is applied on the joints with $x > 0$ for barrel vault and parabolic dome, and with $y > 0$ for hyperbolic paraboloid;
- $Q_{2,2,j}$ is applied on the joints with $x < 0$ for barrel vault and parabolic dome, and with $y < 0$ for hyperbolic paraboloid.

The distributed load q_2 accounts for the weight of glass glazing only.

Structural performance at ULS are evaluated by setting $q_1 = 1800$ N/m^2 and $q_2 = 600$ N/m^2, while SLS performances are assessed with $q_1 = 1200$ N/m^2 and $q_2 = 400$ N/m^2.
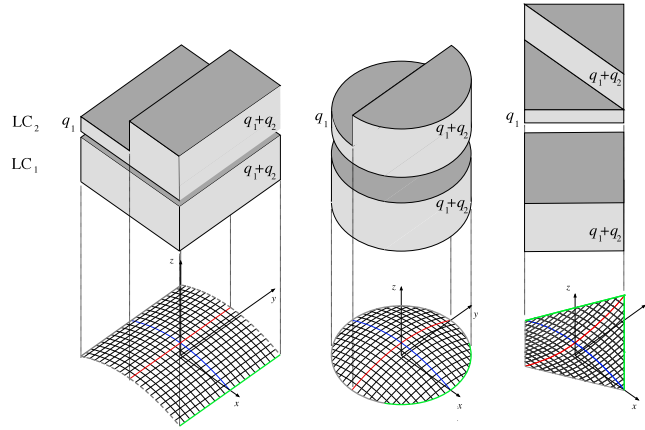
Fig. 7. Load conditions for barrel vault (a), parabolic dome (b) and hyperbolic paraboloid (c).
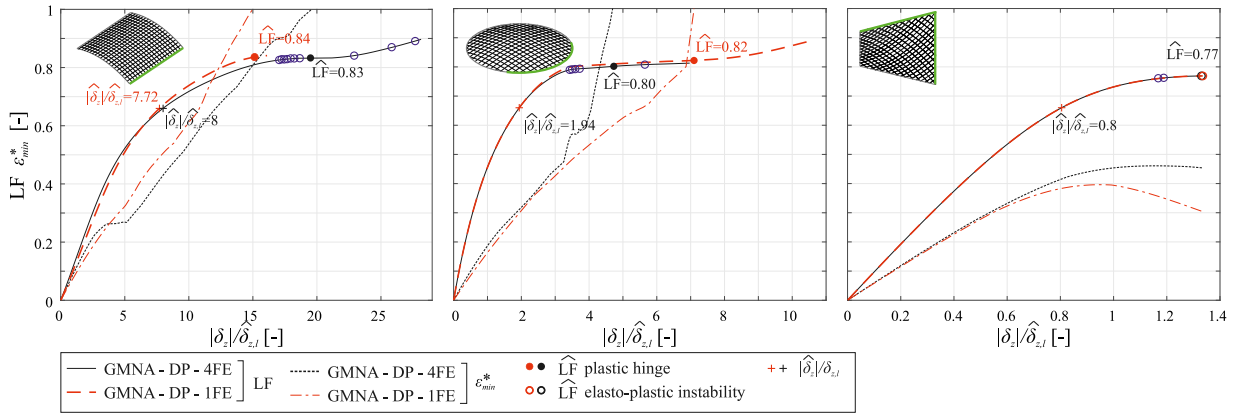

Fig. 8. Effects of the FE discretization of the structural members on the free-edge gridshell structural behaviour.

4. Results

4.1. Effects of the structural modelling assumptions

This section aims to provide a preliminary evaluation of the effects of the structural computational modelling assumptions on the results. In particular, focus is made on two modelling issues that, to the Authors' best knowledge, have not been deeply investigated in the technical literature: i. the discretization of each single structural member into multiple Finite Elements (FEs) to capture the influence of the bending second-order effect and member buckling on the overall gridshell stability, and ii. the plasticity model adopted to capture progressive member yielding.

On the first point, a single FE is adopted per structural member in most of the published studies, e.g. [12,21,81]. Some authors [68,71] discretize each structural member into 4 FEs. Other authors [82] adopt different discretization on the basis of the expected degree of non linearity. However, all the cited studies do not compare the effect of different discretizations on the simulated structural performances. In order to systematically shed light in the issue, Fig. 8 compares, for each free-edge gridshell, the trend of LF and ε_{min}^* versus the dimensionless maximum vertical displacement $|\delta_z|/\hat{\delta}_{z,l}$, obtained by discretizing each structural member into one (1FE) or four Finite Elements (4FE) along its length. Each FE is a Timoshenko beam, also named 'BEAM188' in ANSYS® Mechanical APDL r22.2. Along each load–displacement curve, both the critical load factor $\widehat{LF}$ at ULS and the maximum displacement at SLS load conditions (i.e. LF = 0.66) are highlighted by circular marks (empty or filled depending on the mode of failure) and crosses, respectively. The three gridshells are sensitive to a different extent to the FE discretization: in the hyperbolic paraboloid, FE discretization has negligible effects on the final result at both SLS and ULS; in the parabolic dome, curves do not perfectly overlap, with discretization only slightly influencing $\widehat{LF}$, while providing quite different results in terms of maximum displacement at ULS; in the barrel vault, slight discrepancies emerge both at ULS and SLS, with the largest deviation of the load–displacement curve among the three case studies. These results clearly highlight the importance of multiple FE discretization of each structural member wherever the Ultimate Limit State is preceded and affected by local single-member elasto-plastic instabilities (empty circles in Fig. 8): this is the case of the highly deformable free-edge barrel vault, and of the free-edge parabolic dome to a minor extent.
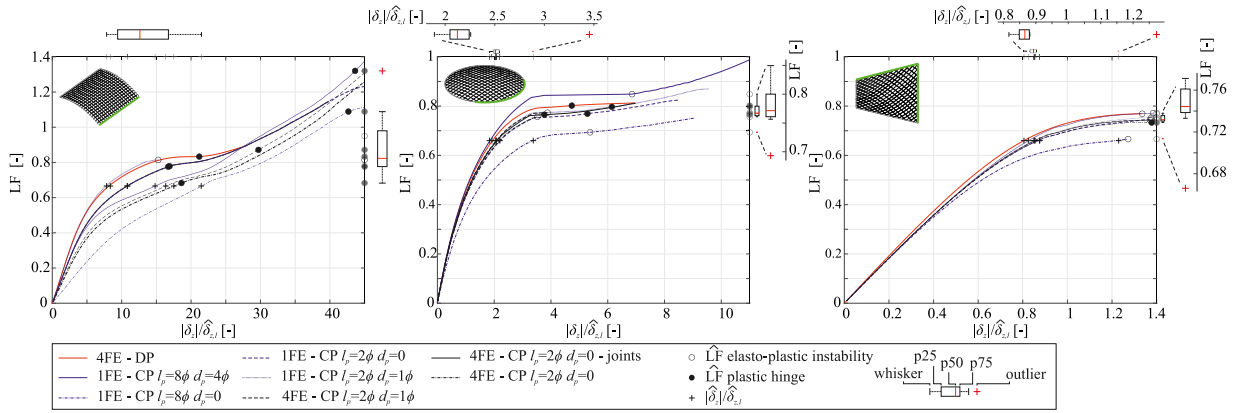
Fig. 9. Effects of the plasticity models on the free-edge gridshell structural behaviour.

Although case-insensitive discretization guidelines cannot be drawn in the light of the above, the 4FE discretization is commonly adopted in the following for all case studies to secure accurate and fully comparable results.

As far as material non-linearities are concerned, a recent report of the IASS WG8 [83] suggests two possible strategies to account for member yielding in gridshells, i.e., the Concentrated Plasticity (CP) model, with multiple discrete plastic hinges located at joints, or the Distributed Plasticity (DP) model. Different authors have adopted one of the two approaches (e.g., [18] for CP, [71] for DP), but comparative studies between them are not available to suggest best practices. In order to contribute to fill such a gap, the load–displacement trends obtained with the DP model and 4FE in ANSYS® Mechanical APDL r22.2 are compared to the ones obtained by adopting the CP model using SAP2000® v21. The adopted plastic hinge type in the latter is the so-called 'Fiber P-M2-M3 Hinge' [64], which is intended to capture the coupled axial normal and biaxial bending behaviour by dividing the cross-section of the element into a series of discrete fibres, each of which has a unique stress–strain relationship based on the assigned material. The axial force–deformation and biaxial moment–rotation of the Timoshenko FE follows from the integration of the behaviour of these fibres across the cross-section and the multiplication by the length of the plastic hinge. The following free parameters are varied in the CP model: structural member discretization (1FE or 4FE); position of the plastic hinge d_p, expressed in terms of distance from the FE nodes; length l_p of the plastic hinge. Both d_p and l_p are normalized with respect to the cross section diameter ϕ. Plastic hinges are located at each FE node, except for one case where they are located only at the structural joints ('joints' label in the following). The values of the CP model free parameters are selected in order to take into account very different modelling choices, even if not systematically. Fig. 9 allows to comparatively discuss the effects of the adopted plasticity model on the structural behaviour of the considered free-edge gridshells. The LF-δ_z curves are visually scattered, particularly for the barrel vault and the parabolic dome, highlighting that their trend is highly sensitive to the free parameters of the CP model. Along each curve, the structural GMs are depicted by different markers, i.e. the critical load factor $\widehat{\text{LF}}$ at ULS and the maximum displacement $|\hat{\delta}_z|$ at SLS. The ensembles of the simulated values of the GMs are projected on the secondary axes, and their synthesis is made by means of boxplots. The coefficient of variation in both $\widehat{\text{LF}}$ and $|\hat{\delta}_z/\hat{\delta}_{z,l}|$ is particularly high for the barrel vault, limited to $\widehat{\text{LF}}$ and much lower than the previous for the parabolic dome, while it is low in $|\hat{\delta}_z|/\hat{\delta}_{z,l}$ for the parabolic dome and in both GMs for the hyperbolic paraboloid. Beyond the GMs, CP model parameters also affect the overall mode of failure, switching from elasto-plastic instability to plastic hinge formation, and vice-versa, as highlighted by empty and filled circular markers, respectively. None of the tested CP models allows to perfectly match the results obtained with the DP model. However, the obtained load–displacement curve is reasonably in agreement with the one obtained with the DP model when plastic regions are placed at the structural joints only and their length set equal to 2ϕ. In the following, the DP model is preferred to the CP one in order to avoid the dispersion of the results induced by the CP model free parameters.

These preliminary analyses, even though not exhaustive, provide a first reference background to support the adopted modelling choices. The Authors hope that such a preliminary study will pave the way towards future ones within the FreeGrid benchmark to increase the cardinality of the simulated results, so to allow a more accurate and systematic uncertainty quantification.

4.2. Structural performances

Before discussing the structural Design Goal and Performance metrics of fully-constrained gridshells with respect to free-edge ones, a comprehensive reading of the structural behaviour of both kind of structures is outlined in Figs. 10 to 13.

Fig. 10 provides an overview of the normalized joint displacements at SLS along normal and tangential directions for all the analysed gridshell structures. For each geometry and boundary condition (fully-constrained or free-edge, highlighted in green), displacements are scaled with respect to the modulus of the maximum nodal displacement $|\hat{\delta}|$ obtained from both Load Conditions. In the figure, circle dimensions are proportional to the scaled joint displacements. Moreover, for the orthogonal components, black and grey dots refer to downward and upward displacement, respectively. The following considerations can be outlined:
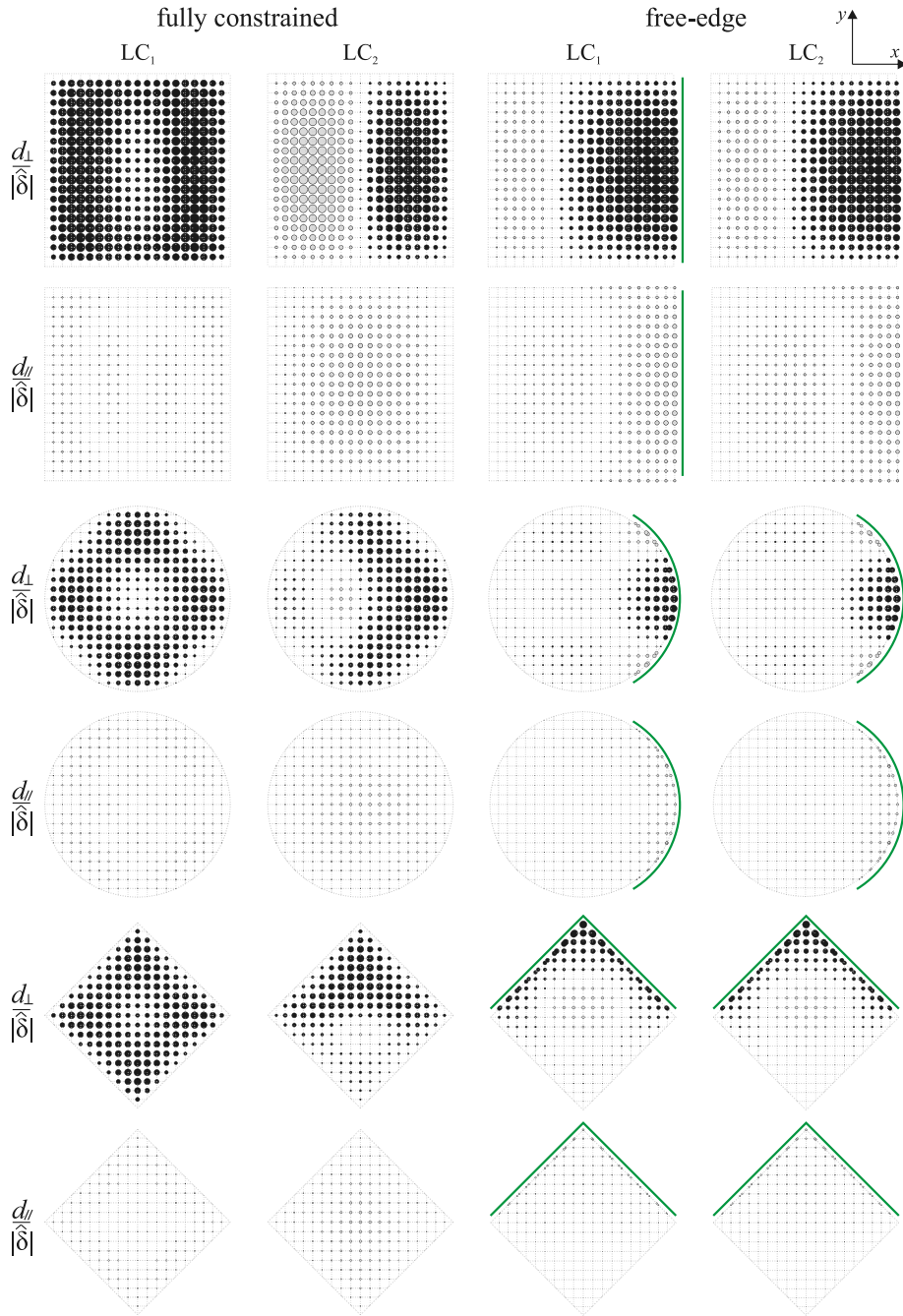
Fig. 10. Joint displacements along orthogonal and tangential directions in fully-constrained and free-edge gridshells at SLS.

- the largest normal displacements are concentrated in the area between the hinged spring line and the axes origin in fully constrained gridshells, while they are clustered close to the free edge in free-edge gridshells;
- in general, the normal component prevails on the tangential one. The only exception occurs for the barrel vault, where the tangential component of displacement is not negligible in the case of free-edge gridshell and fully-constrained gridshell subjected to LC_2;
- in the fully-constrained gridshells, different load conditions correspond to quite different displacement patterns. Conversely, in the free-edge gridshells, the effect induced by the free edge on the displacement field prevails over the one induced by the load condition, resulting in asymmetric displacement patterns also for symmetric loads.
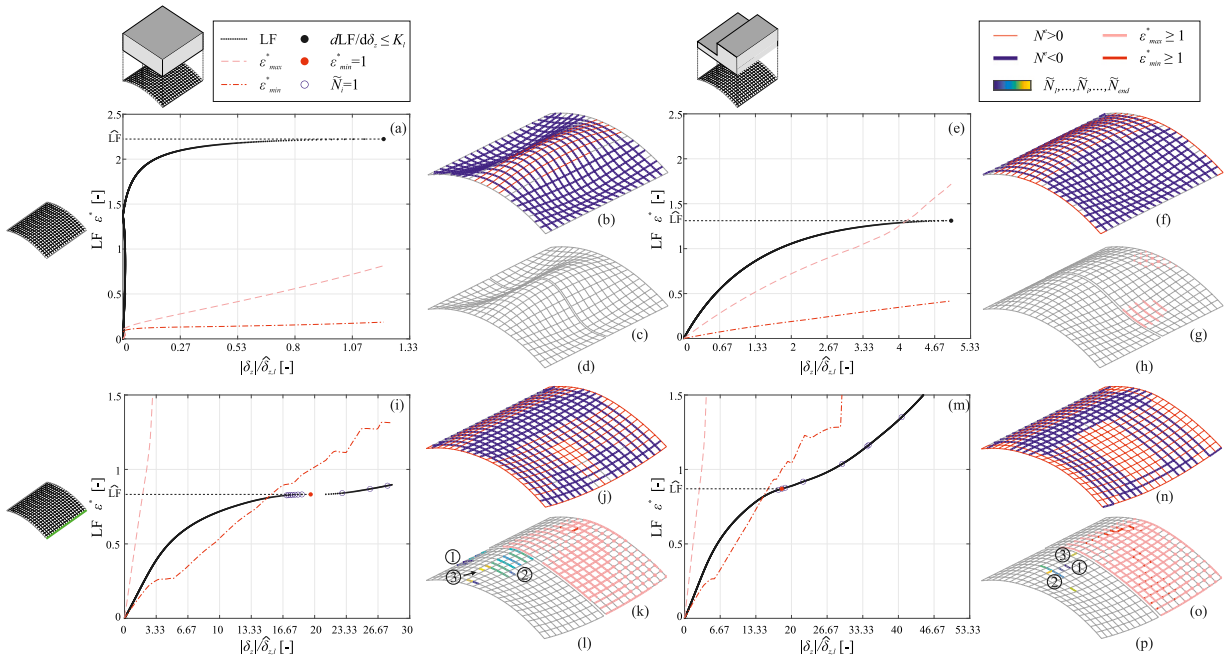
Fig. 11. Barrel vault structural performance: assessment of $\widehat{LF}$, ε^*_{max} and ε^*_{min} curves (a,e,i,m); members under tension and compression (b,f,j,n); yielded FE for which $\varepsilon^*_{max} \geq 1$ and $\varepsilon^*_{min} \geq 1$ (c,g,k,o); and members subjected to progressive buckling (d,h,l,p) over gridshell deformed shape at ULS.

The above considerations suggest that:

- the strong differences in the distribution of normal and tangential displacements over the gridshells surfaces highlight that the mechanical resistant working principles change significantly among the three tested geometries and strongly depend on the boundary condition;
- SLS performances of free-edge gridshells can be improved by design strategies aimed at stiffening the free edge in the normal direction.

Figs. 11–13 organize the obtained results necessary for the determination of $\widehat{LF}$ in a 2×2 matrix of subgraphs. Rows correspond to constraint conditions, i.e. fully-constrained or free-edge, while columns correspond to load conditions, i.e. LC_1 and LC_2. Results for each setup are condensed in a diagram plotting LF, ε^*_{max} and ε^*_{min} curves over the maximum dimensionless nodal vertical displacement $|\delta_z|/\hat{\delta}_{z,l}$. Alongside the diagram, the distributions of members under tension and compression, groups of yielded FE for which $\varepsilon^*_{max} \geq 1$ and $\varepsilon^*_{min} \geq 1$, and members that progressively buckles are highlighted over the gridshell deformed shape at ULS, to shed some light on the resistant working principle of the gridshells. For the sake of clarity, groups of members attaining progressive buckling are numbered sequentially in Figs. 11(l,p), 12(k,o) and 13(d,h).

Overall, the free edge modifies the resistant working principle of gridshells from a characteristic membrane mechanical behaviour to a mixed membrane-flexural behaviour. However, the analysed case studies show that the free edge has different effects on the resistant working principle of gridshell structures, depending on their geometry. Concerning the barrel vault and parabolic dome, the free edge increases the amount of members subjected to tension and increases the amount of partially plasticized members at ULS. In particular, the free-edge parabolic dome concentrates plasticization along members close to the boundaries of the free-edge, while the free-edge barrel vault spread plasticization on a larger amount of members, because of its single curvature. Concerning the hyperbolic paraboloid, the free edge does not alter its overall resistant working principle, maintaining a prevailing membrane behaviour. Specific and detailed comments on each structure follow.

In the fully-constrained barrel vault (Fig. 11b,f), the members of the *x*-wise arches are mainly subjected to compression, while members along the *y*-wise direction are subjected to tension or compression depending on the load condition. In the free-edge barrel vault (Fig. 11j,n), *x*-wise compressed members are reduced with respect to the fully-constrained geometry. The asymmetric load condition further reduces the amount of *x*-wise compressed members while increasing the amount of *x*-wise and *y*-wise members subjected to positive normal stress in proximity of the free edge. The fully-constrained barrel vault displays a quite different mechanical behaviour depending on the load condition, with much higher critical LF in the case of symmetric loading (Fig. 11a,e). On the other hand, the free-edge gridshell displays a mechanical behaviour weakly dependent on load conditions, reaching similar values of the critical LF (Fig. 11i,m). In particular, the fully-constrained barrel vault subjected to uniform load reaches global instability within a fully elastic regime contextually to lower overall displacements. Conversely, the asymmetrical load anticipates the overall instability of the gridshell, despite entering within the elasto-plastic regime. Some sections partially
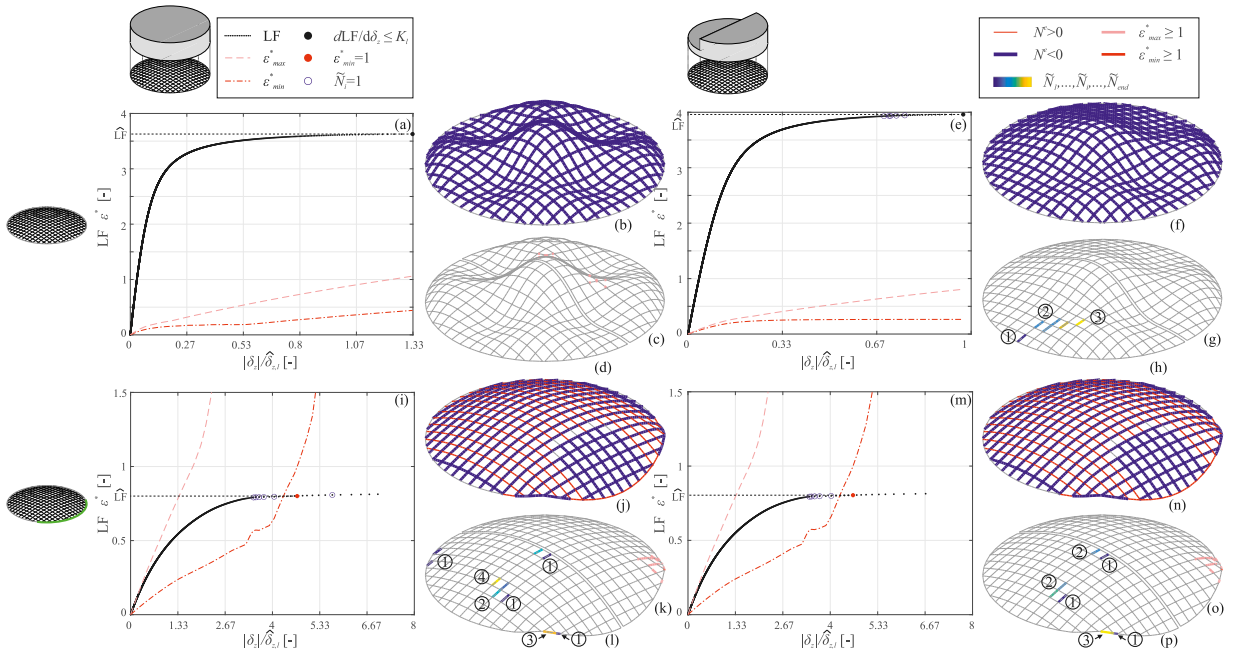
Fig. 12. Parabolic dome structural performance: assessment of $\widehat{LF}$, ε^*_{max} and ε^*_{min} curves (a,e,i,m); members under tension and compression (b,f,j,n); yielded FE for which $\varepsilon^*_{max} \geq 1$ and $\varepsilon^*_{min} \geq 1$ (c,g,k,o); and members subjected to progressive buckling (d,h,l,p) over gridshell deformed shape at ULS.

plasticize and mainly concentrate along the x-wise members with larger bending, and in the x- and y-wise members on the top of the barrel vault in proximity of the end arches (Fig. 11g). The free-edge barrel vault reaches cross-section yielding and formation of plastic hinges before reaching overall instability for both load conditions (Fig. 11k,o). In particular, progressive member instability slightly anticipate the formation of plastic hinges. Member buckling takes place and mainly localizes along the x-wise arches for both load conditions (Fig. 11l,p). However, it first occurs close to the spring-lines and then close to the top of the arch when the load is symmetric, while it remains centred close to the top when the load is asymmetric.

The mechanical behaviour of the fully constrained parabolic dome is independent of the load condition. Indeed, all members are under compression (Fig. 12b,f) and the LF trend looks analogous (Fig. 12a,e). However, LC_1 anticipates the partial plasticization of the members (Fig. 12c), being $\varepsilon^*_{max} \geq 1$ at ULS, while LC_2 induces the progressive buckling in proximity of the load discontinuity ($x = 0$), from the members close to the spring line towards the free-edge (Fig. 12h). Contrarily to the fully-constrained barrel vault, the critical load factor is reached within the elastic regime when the load is asymmetric, while it is reached within the elasto-plastic regime when the load is symmetric. Furthermore, LC_2 causes the counter-intuitive slight increase of $\widehat{LF}$. The free edge switches the vast majority of members in x-wise arches from compression to tension, except for the ones located in proximity of the free-edge (Fig. 12j,n). The free-edge dome behaves almost identically whichever the load condition, and reaches $\widehat{LF}$ in the wake of progressive member buckling and the formation of plastic hinges (Fig. 12i,m). Cross-sections partial plasticization and occurrence of plastic hinges concentrate in correspondence of the boundaries of the free edge, where members are subjected to large rotations (Fig. 12k,o). Conversely, progressive buckling propagates from members of y-wise arches in proximity of $x = 0$ at the top and close to the reins to members of the free-edge (Fig. 12l,p).

The hyperbolic paraboloid shows a quite different mechanical behaviour with respect to the previous cases. Indeed, the negative Gaussian curvature implies that structural members along the y direction are always in tension, regardless of the load and constraint conditions (see Fig. 13b,f,j,n). In the fully-constrained hyperbolic paraboloid, LC_2 causes the stresses of x-wise members directly loaded by q_1 ($y < 0$) to switch form compression to tension (Fig. 13b,f). The critical load factor is reached within the elasto-plastic regime for both load conditions (Fig. 13a,e). However, the partial plasticization of cross-sections occurs in different portions of the gridshell: through the whole central strip of the gridshell for LC_1, while it concentrates on the side where the applied load is higher for LC_2 (Fig. 13c,g). Furthermore, progressive buckling involves x-wise members over the whole gridshell for LC_1, from the centre ($y = 0$) to the sides ($y \approx \pm B/2$), while it concerns a limited number of x-wise members for LC_2, from the centre to the side supporting the higher load ($y \approx -B/2$) (Fig. 13d,h). The free edge only affects the members along it, switching from almost nil to negative stress (Fig. 13j,n). Although the load condition affects the sign of the stress of the x-wise members for $y < 0$, the difference in the overall resistant working principles is negligible. Indeed, the free-edge hyperbolic paraboloid behaves likewise whichever the load condition and reaches $\widehat{LF}$ within the elasto-plastic regime (Fig. 13i,m) in the wake of the buckling of a few members in the compressed free-edge (Fig. 13l,p).

Fig. 14 summarizes the structural Goal Metrics for all the gridshells. The following synthetic comments can be outlined:
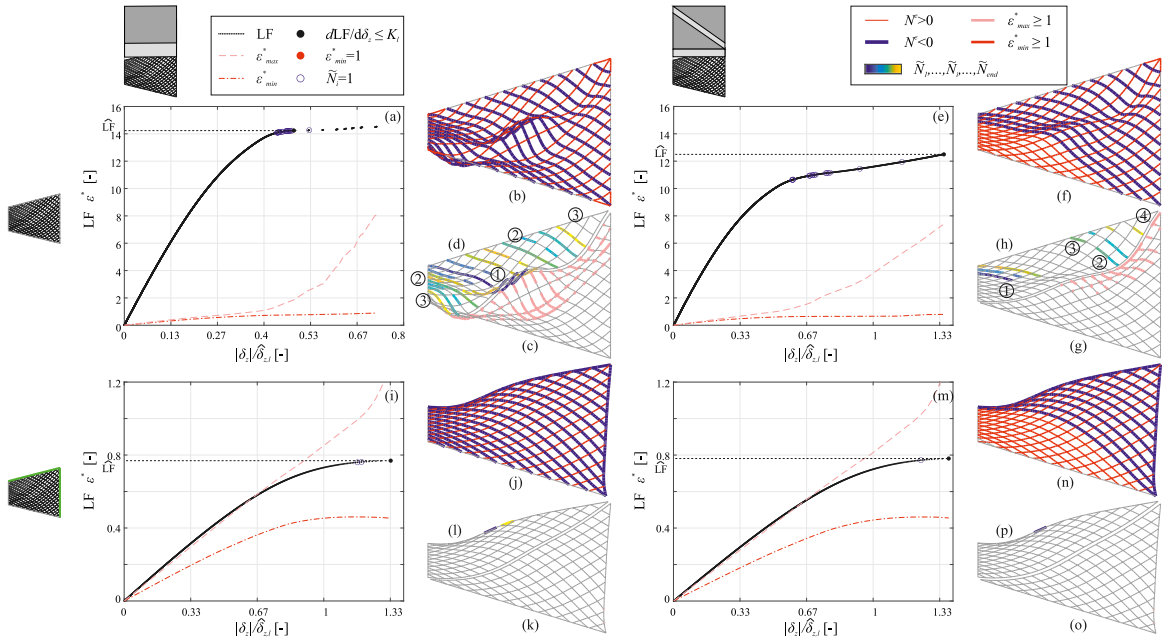
Fig. 13. Hyperbolic paraboloid structural performance: assessment of $\widehat{\text{LF}}$, ε^*_{max} and ε^*_{min} curves (a,e,i,m); members under tension and compression (b,f,j,n); yielded FE for which $\varepsilon^*_{max} \geq 1$ and $\varepsilon^*_{min} \geq 1$ (c,g,k,o); and members subjected to progressive buckling (d,h,l,p) over gridshell deformed shape at ULS.
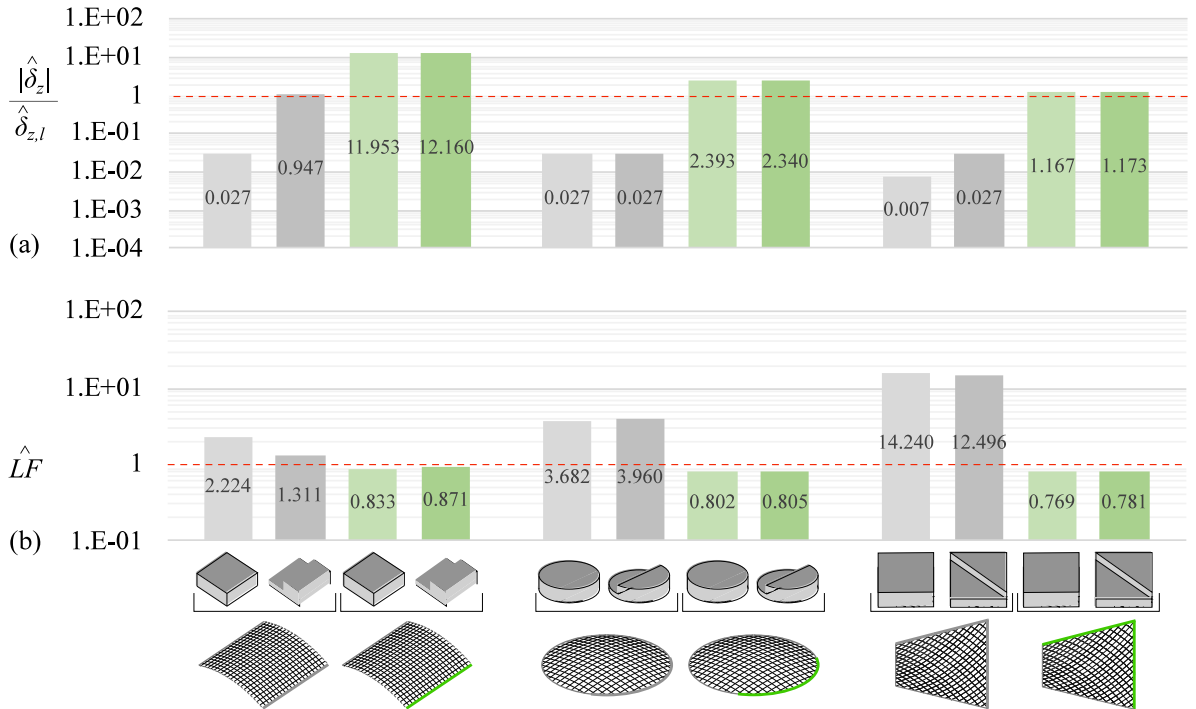

Fig. 14. Structural GM for all gridshells and Load Conditions: Dimensionless vertical displacements at SLS (a); critical Load Factor (b).

• In general terms, the bulk effects of the dissymmetry induced by the free-edge constraint condition largely prevails over the ones of the asymmetric load condition. In spite of this common general trend, the effects of different load conditions on the maximum vertical displacement and critical load factor slightly vary with the geometry of the gridshells. Double curvature gridshells (i.e. both parabolic dome and hyperbolic paraboloid) ensure that structural performances do not dramatically change
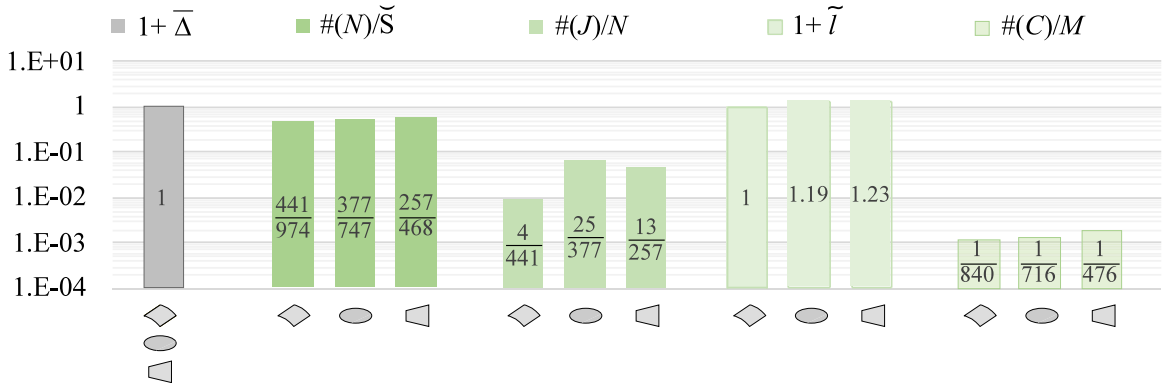
Fig. 15. Buildability Goal Metrics: normalized values of out-of-planarity of faces $\bar{A}$, joint number $\#(N)$, cardinality of the ensembles of joint types $\#(J)$, coefficient of variation of members length $\bar{l}$, and cardinality of the ensembles of members cross sections types $\#(C)$.
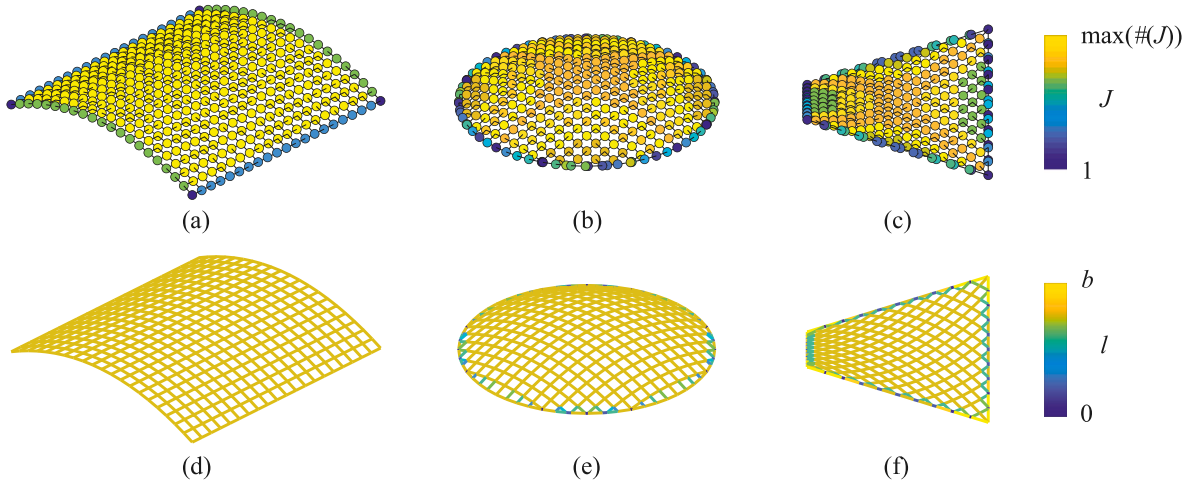

Fig. 16. Buildability Goal Metrics: joint type J (a,b,c) and member length l (d,e,f).

under different load condition for both fully and partially constrained cases. An analogous response holds for the partially constrained barrel vault, where the effects of the free edge largely outweigh the ones induced by load conditions. Conversely, the fully constrained single curvature barrel vault is very sensitive to the asymmetric load case LC_2 that proves to be most demanding condition at both SLS and ULS.

- All free-edge gridshells do not satisfy performance levels at both SLS ($|\hat{\delta}_z|/\hat{\delta}_{z,l} > 1$) and ULS ($\widehat{LF} < 1$), while fully-constrained gridshells do.
- Fully-constrained gridshells dramatically increase the structural performances of all geometries at both ULS and SLS: the critical load factors of the fully-constrained gridshells are from 2 to 20 times higher than the ones of the corresponding free-edge ones; the maximum vertical displacements of the fully-constrained gridshells are from 13 to 440 times lower than the ones of the corresponding free-edge ones. In particular, the hyperbolic paraboloid is the gridshell with the highest difference in terms of $\widehat{LF}$ under both load conditions, while the barrel vault is the most sensitive in terms of $|\hat{\delta}_z|$, namely under uniform LC_1.
- $\widehat{LF}$ approximately takes the same value for all free-edge gridshells.
- Conversely, the free-edge gridshells perform differently at SLS, in the light of their geometrical (i.e., simple or double curvature) and mechanical (i.e., structural members in tension or compression) specific features. In particular, the free-edge barrel vault, due to its single curvature, is particularly sensitive to serviceability issues: $|\hat{\delta}_z|/\hat{\delta}_{z,l} \approx 12$ under both load conditions. Free-edge parabolic dome ($|\hat{\delta}_z|/\hat{\delta}_{z,l} \approx 2.4$) and free-edge hyperbolic paraboloid ($|\hat{\delta}_z|/\hat{\delta}_{z,l} \approx 1.2$) are increasingly stiffer.

4.3. Buildability performances

According to the features of the adopted case studies, both buildability and sustainability Goal Metrics have the same values for free-edge and fully-constrained gridshells. Fig. 15 summarizes the buildability Goal Metrics for all the gridshells, while variability
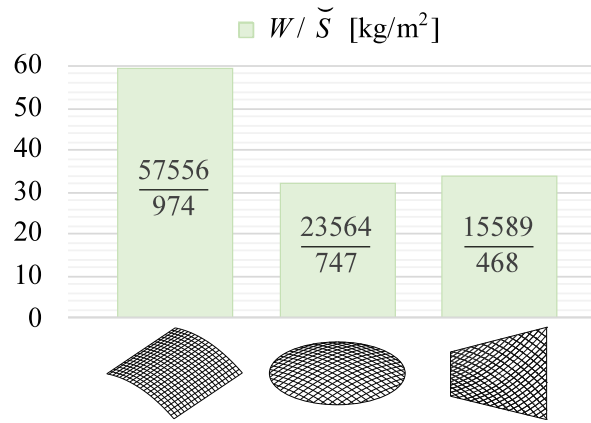
Fig. 17. Sustainability Goal Metric: normalized values of the equivalent weight W.

of member length and joint types is represented in detail over the gridshells surfaces in Fig. 16. The following synthetic comments can be outlined:

- Out-of-planarity of the gridshell faces is nil since all quadrangular square faces are planar, resulting from discrete translational surfaces, i.e., obtained from the translation of a discrete parabolic generatrix over a discrete directrix. Both the generatrix and the directrix are homogeneously decomposed into all-equal segments.
- The barrel vault contains the largest cardinality of structural joints while the hyperbolic paraboloid contains the lowest one. This is mainly related to the gridshell surface $\check{S}$ of each gridshell that is maximum for the barrel vault and minimum for the hyperbolic paraboloid. However, surface density of the joints is not constant, despite the mesh uniformity. It ranges within $\#(N^*) \in [0.45, 0.55]$, with the hyperbolic paraboloid scoring the highest value, because of the high surface density of joints resulting from the intersection of the gridshell internal members with the members along the spring line.
- Uniformity in structural joints varies sensibly among the three gridshells, even if they all share the same positive x-wise curvature and the parabolic dome and hyperbolic paraboloid also share the same absolute value of the y-wise curvature. Fig. 16(a,b,c) highlights that non-uniformity in structural joints rises because of the intersection of internal members with members arranged along the spring line. The barrel vault scores the lowest cardinality of joint types because its boundary is perfectly aligned with the grid of members. Conversely, the parabolic dome scores the highest cardinality of joint types because the grid intersect the spring line at different heights.
- Uniformity in members length slightly varies among the three gridshells, despite their uniform quadrangular square faces. The barrel vault is perfectly uniform, having all members with the same length $l = b$. Fig. 16(d,e,f) highlights that non-uniformity in members of the parabolic dome and hyperbolic paraboloid is triggered by the triangular faces resulting from the non-boundary fitted mesh alongside the spring line.
- Non-uniformity in member cross-sections is similar for the barrel vault and parabolic dome, since they have similar number of structural members. Conversely, it almost doubles for the hyperbolic paraboloid since the number of members M is almost halved.

4.4. Sustainability performances

Fig. 17 summarizes the single sustainability Goal Metric for all the gridshells.

In this case study, sustainability performance is directly related to the grid density and the gridshell total weight, since the steel grade and the type of member cross-section are the same among the three design solutions. On the one hand, gridshell weight is directly proportional to the cross-section area of the structural members and the gridshell surface $\check{S}$. On the other hand, grid density is almost constant among the three gridshells and slightly increases approaching the boundaries for the parabolic dome and hyperbolic paraboloid. The barrel vault scores the highest normalized equivalent weight among the three solutions and about equal to two times the value of the parabolic dome and more than three times the value of the hyperbolic paraboloid. This is because of the double cross-section area of its members with respect to the other design solutions. The parabolic dome and hyperbolic paraboloid reach about the same normalized equivalent weight since they share the same cross section.

4.5. Bulk performance

Goal Metrics of the fully-constrained gridshells are made dimensionless by referring to free-edge gridshells baseline design solution. Dimensionless structural, buildability and sustainability GMs are summarized in Fig. 18. In particular, structural GMs are referred to uniform and asymmetric load conditions.
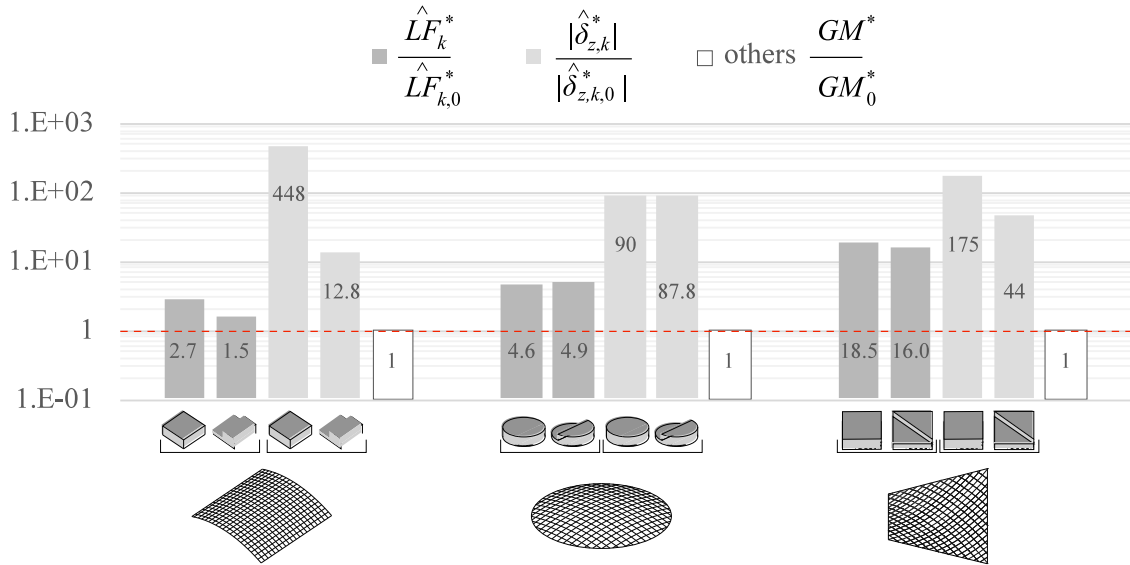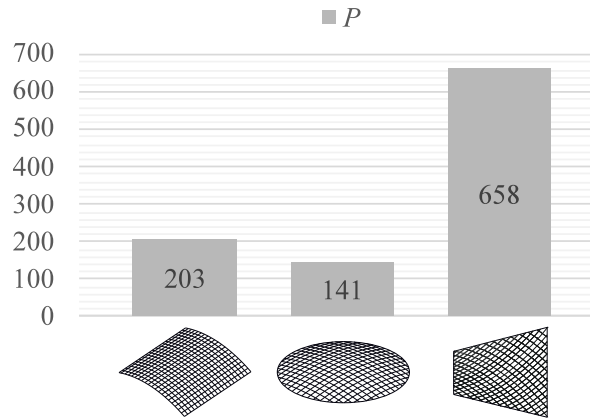
Fig. 18. Dimensionless Goal Metrics.

Fig. 19. Bulk Performance metrics P.

As expected, structural GMs increase, while buildability and sustainability GMs are not affected by the restraint applied along the gridshells edge. The increment of structural performance at ULS and SLS varies depending on both the load condition and the gridshell geometry. In general, the asymmetric load conditions gives rise to lower dimensionless GMs with respect to the symmetric load counterparts. However, the parabolic dome is the least sensitive to the load condition, and it even induces a higher dimensionless critical load factor when the load is asymmetrically distributed. Conversely, the barrel vault is the most susceptible to variations in the load condition. Dimensionless SLS GMs are one order of magnitude higher than ULS GMs. Indeed, dimensionless critical load factors range from 2 to 19, while dimensionless vertical displacements range from 13 to 448. This testifies the large susceptibility of the baseline design solutions to free-edge vertical displacements.

Finally, the Bulk Performance metrics of the fully constrained gridshells are evaluated with respect to the baseline free-edge ones and summarized in Fig. 19. BP metrics are directly related to structural Partial Performance ones, since buildability and sustainability ones result equal to unit. The histogram highlights that the fully-constrained hyperbolic paraboloid scores the highest BP. This is induced by (i) the extent of the free edge, i.e. the largest one among the three geometries together with the barrel vault, and (ii) the inborn high structural performance of the hyperbolic paraboloid geometry, taking advantage of arches under compression and rods under tensions arranged along the two principal directions. Conversely, the parabolic dome scores the lowest BP. On the one side, the extent of the free edge is the shortest among the baseline design solutions, and its restraining does not dramatically change its overall structural performance. On the other side, the double curvature allow the free-edge parabolic dome to perform significantly better than the free-edge barrel vault at SLS.

5. Conclusions and perspectives

This study provides a detailed insight on a methodological framework for the holistic performance assessment of steel, single-layer gridshells. The performance assessment is intended to: i. be conceptual design oriented and supportive by referring to design goals; ii. analytically consider multiple design goals, each expressed by a quantitative goal metric; iii. secure the direct comparison in absolute terms of each goal metric among multiple design solutions to different design problems thanks to their suitable normalization; iv. consider three different types of performances, namely the structural, buildability and sustainability ones; v. make synthesis of them in a bulk performance metric by making the partial ones homogeneous and dimensionless; vi. allow the comparison of the bulk performance of several design solutions even if all referred to a single design problem by necessarily making reference to a guessed baseline design solution.

The desired beneficial original contribution of this study is threefold. First, the analytical form of the method is meant to be directly applicable by future researchers and engineers (i) within the design phase as objective function in optimization algorithms so as to develop methodologies able to holistically increment structural, buildability and sustainability performances and (ii) in a post-design phase to retrieve a synthetic index of the overall gridshell performance able to effectively compare among them different design solutions and/or different design approaches. Secondly, the study clarifies the till now scarcely studied structural behaviour of different free-edge gridshells, also with respect to their fully constrained counterparts. Thirdly, the proposed method is applied to the three Design Baseline Gridshells adopted by the FreeGrid benchmark [57]. In the FreeGrid perspective, the outcomes of the present study are meant to provide to participants an in-depth, common background knowledge about the baseline structures, so as to be inspirational for design solutions improving their overall performances.

According to the Authors, the study offers multiples short-term research and development perspectives to the scientific and technical community. First, the proposed framework is general, flexible and open in its conceptual architecture, so that it is potentially ready to be adapted and/or expanded to deal with different types of structures (e.g., continuous shells, bending active gridshells), structural materials (e.g. wood, reinforced concrete), types of mechanical models (e.g., linear buckling analysis, modal analysis), dynamic loads (e.g. induced by wind [84], earthquake [85], blast [86]), design stages. Such extensions may need the tuning of specific coefficients (e.g., the environmental impact correction coefficient), the redefinition of some goal metrics (e.g., the Load Factor as obtained by a linear buckling analysis), the addition of further goal metrics (e.g., the ones relevant to the mechanical performance of the structure face to dynamic loads, or the buildability of the structural joints in the detailed design stage). Second, the newborn FreeGrid benchmark will offer the opportunity to further test the method at work with reference to the variety of proposed design solutions, and that will presumably differ in both their geometrical and structural features. Such an extensive benchmarking will allow to further test the soundness of the approach allowing for an extensive calibration and possible extensions.

CRediT authorship contribution statement

Lorenzo Raffaele: Writing – review & editing, Writing – original draft, Visualization, Methodology, Investigation, Formal analysis, Data curation, Conceptualization. **Luca Bruno:** Writing – review & editing, Writing – original draft, Visualization, Supervision, Project administration, Methodology, Investigation, Conceptualization. **Francesco Laccone:** Writing – review & editing, Writing – original draft, Visualization, Investigation, Formal analysis, Data curation, Conceptualization. **Fiammetta Venuti:** Writing – review & editing, Writing – original draft, Methodology, Investigation. **Valentina Tomei:** Writing – review & editing, Writing – original draft, Investigation, Software, Formal analysis.

Declaration of competing interest

The authors declare that they have no known competing financial interests or personal relationships that could have appeared to influence the work reported in this paper.

Data availability

The geometrical models (in dxf and obj formats) and the mechanical models (as ASCII input files for Ansys Mechanical APDL 22.2) of the Design Baseline Gridshells studied in the paper are available in Open Access at the web site of the FreeGrid benchmark https://sites.google.com/view/freegrid/data-tools), together with post-processing tools (in python and xlsx format) for the assessment of the bulk and partial performance metrics.

Acknowledgements

References

[1] M. Beckh, R. Barthel, The first doubly curved gridshell structure - Shukhovs building for the plate rolling workshop in Vyksa, in: Proceedings of the Third International Congress on Construction History, Cottbus, 2009.

[2] F. Otto, E. Shauer, J. Hennicke, IL 10 Gitterschalen / Grid Shells, Institute fur Leichte Flachentragwerke, Stuttgart, 1974.

[3] R. Fuller, J. Ward, The Artifacts of R. Buckminster Fuller: A Comprehensive Collection of His Designs and Drawings, Garland, 1985.

[4] I. Liddell, Frei Otto and the development of gridshells, Case Stud. Struct. Eng. 4 (2015) 39–49, http://dx.doi.org/10.1016/j.csse.2015.08.001.

[5] J. Schlaich, H. Schober, Glass-covered grid-shells, Struct. Eng. Int. 6 (2) (1996) 88–90, http://dx.doi.org/10.2749/101686696780495716.

[6] H. Schober, Transparent Shells: Form, Topology, Structure, John Wiley & Sons, 2015.

[7] J. Chilton, G. Tang, Timber Gridshells: Architecture, Structure and Craft, Routledge, 2017.

[8] D. Rockwood, Bamboo Gridshells, Routledge, 2015.

[9] F. Tayeb, J.-F. Caron, O. Baverel, L.D. Peloux, Stability and robustness of a 300m^2 composite gridshell structure, Constr. Build. Mater. 49 (2013) 926–938, http://dx.doi.org/10.1016/j.conbuildmat.2013.04.036.

[10] S. Dyvik, B. Manum, A. Rønnquist, Gridshells in recent research-a systematic mapping study, Appl. Sci. 11 (2021) 11731, http://dx.doi.org/10.3390/app112411731.

[11] V. Gioncu, Buckling of reticulated shells: State-of-the-art, Int. J. Space Struct. 10 (1) (1995) 1–46, http://dx.doi.org/10.1177/026635119501000101.

[12] T. Bulenda, J. Knippers, Stability of grid shells, Comput. Struct. 79 (2001) 1161–1174, http://dx.doi.org/10.1016/S0045-7949(01)00011-6.

[13] J. Cai, L. Gu, Y. Xu, J. Feng, J. Zhang, Nonlinear stability analysis of hybrid grid shells, Int. J. Struct. Stab. Dyn. 13 (1) (2013) 1–16, http://dx.doi.org/10.1142/S0219455413500065.

[14] F. Fan, Z. Cao, S. Shen, Elasto-plastic stability of single-layer reticulated shells, Thin-Walled Struct. 48 (2010) 827–836, http://dx.doi.org/10.1016/j.tws.2010.04.004.

[15] S. Malek, T. Wierzbicki, J. Ochsendorf, Buckling of spherical cap gridshells: A numerical and analytical study revisiting the concept of the equivalent continuum, Eng. Struct. 75 (15) (2014) 288–298, http://dx.doi.org/10.1016/j.engstruct.2014.05.049.

[16] D. Tonelli, N. Pietroni, E. Puppo, M. Froli, P. Cignoni, G. Amendola, R. Scopigno, Stability of statics aware Voronoi grid-shells, Eng. Struct. 116 (2016) 70–82, http://dx.doi.org/10.1016/j.engstruct.2016.02.049.

[17] C. Borri, P. Spinelli, Buckling and post-buckling behavior of reticulated shells affected by random imperfections, Comput. Struct. 30 (4) (1988) 937–943, http://dx.doi.org/10.1016/0045-7949(88)90131-9.

[18] S. Kato, I. Mutoh, M. Shomura, Collapse of semi-rigidly jointed reticulated domes with initial geometric imperfections, J. Constr. Steel Res. 48 (1998) 145–168, http://dx.doi.org/10.1016/S0143-974X(98)00199-0.

[19] S. Yamada, A. Takeuchi, Y. Tada, K. Tsutsumi, Imperfection-sensitive overall buckling of single-layer lattice domes, J. Eng. Mech. 127 (2001) 382–386, http://dx.doi.org/10.1061/(ASCE)0733-9399(2001)127:4(382).

[20] J. Guo, Research on distribution and magnitude of initial geometrical imperfection affecting stability of suspen-dome, Adv. Steel Constr. 7 (4) (2011) 344–358, http://dx.doi.org/10.18057/IJASC.2011.7.4.3.

[21] L. Bruno, M. Sassone, F. Venuti, Effects of the equivalent geometric nodal imperfections on the stability of single layer grid shells, Eng. Struct. 112 (2016) 184–199, http://dx.doi.org/10.1016/j.engstruct.2016.01.017.

[22] V. Tomei, E. Grande, M. Imbimbo, Influence of geometric imperfections on the efficacy of optimization approaches for grid-shells, Eng. Struct. 228 (2021) 111502, http://dx.doi.org/10.1016/j.engstruct.2020.111502.

[23] E. Fathelbab, The Effect of Joints on the Stability of Shallow Single Layer Lattice Domes (Ph.D. thesis), University of Cambridge, 1987.

[24] K.-J. Hwang, J. Knippers, S.-W. Park, Influence of various types node connectors on the buckling loads of grid shells, in: IASS Symposium, 2009.

[25] H. Ma, F. Fan, P. Wen, H. Zhang, S. Shen, Experimental and numerical studies on a single-layer cylindrical reticulated shell with semi-rigid joints, Thin-Walled Struct. 86 (2015) 1–9, http://dx.doi.org/10.1016/j.tws.2014.08.006.

[26] L. Bruno, F. Venuti, Influence of in-plane and out-of-plane stiffness on the stability of free-edge gridshells: A parametric analysis, Thin-Walled Struct. 131 (2018) 755–768, http://dx.doi.org/10.1016/j.tws.2018.07.019.

[27] R. Harris, J. Romer, O. Kelly, S. Johnson, Design and construction of the Downland gridshell, Build. Res. Inf. 31 (6) (2003) 427–454, http://dx.doi.org/10.1080/0961321032000088007.

[28] F. Laccone, L. Malomo, N. Pietroni, P. Cignoni, T. Schork, Integrated computational framework for the design and fabrication of bending-active structures made from flat sheet material, Structures 34 (2021) 979–994, http://dx.doi.org/10.1016/j.istruc.2021.08.004.

[29] Y. Liu, T. Lee, A. Koronaki, N. Pietroni, Y. Xie, Reducing the number of different nodes in space frame structures through clustering and optimization, Eng. Struct. 284 (116016) http://dx.doi.org/10.1016/j.engstruct.2023.116016.

[30] X. Tellier, C. Douthe, L. Baverel, O. Baverel, Caravel meshes: A new geometrical strategy to rationalize curved envelopes, Structures 28 (2020) 1210–1228, http://dx.doi.org/10.1016/j.istruc.2020.09.033.

[31] J. Schlaich, H. Schober, Glass roof for the hippo house at the Berlin Zoo, Struct. Eng. Int. 7 (4) (1997) 252–254, http://dx.doi.org/10.2749/101686697780494581.

[32] H. Pottmann, Y. Liu, J. Wallner, A. Bobenko, W. Wang, Geometry of multi-layer freeform structures for architecture, in: ACM SIGGRAPH 2007 Papers, SIGGRAPH '07, Association for Computing Machinery, New York, NY, USA, 2007, pp. 65–es, http://dx.doi.org/10.1145/1275808.1276458.

[33] Y. Liu, W. Xu, J. Wang, L. Zhu, B. Guo, F. Chen, G. Wang, General planar quadrilateral mesh design using conjugate direction field, ACM Trans. Graph. 30 (6) (2011) 1–10, http://dx.doi.org/10.1145/2070781.2024174.

[34] C. Jiang, C. Wang, X. Tellier, J. Wallner, H. Pottmann, Planar panels and planar supporting beams in architectural structures, ACM Trans. Graph. 42 (2) http://dx.doi.org/10.1145/3561050.

[35] C. Wang, C. Jiang, H. Wang, X. Tellier, H. Pottmann, Architectural structures from quad meshes with planar parameter lines, Comput. Aided Des. 156 (2023) 103463, http://dx.doi.org/10.1016/j.cad.2022.103463.

[36] M. Eigensatz, M. Kilian, A. Schiftner, N.J. Mitra, H. Pottmann, M. Pauly, Paneling architectural freeform surfaces, in: ACM SIGGRAPH 2010 Papers, SIGGRAPH '10, Association for Computing Machinery, New York, NY, USA, 2010, http://dx.doi.org/10.1145/1833349.1778782.

[37] H. Wang, D. Pellis, F. Rist, H. Pottmann, C. Müller, Discrete geodesic parallel coordinates, ACM Trans. Graph. 38 (6) http://dx.doi.org/10.1145/3355089.3356541.

[38] D. Pellis, M. Kilian, H. Pottmann, M. Pauly, Computational design of Weingarten surfaces, ACM Trans. Graph. 40 (4) (2021) 1–11, http://dx.doi.org/10.1145/3450626.3459939.

[39] R. Mesnil, C. Douthe, O. Baverel, B. Léger, J. Caron, Isogonal moulding surfaces: A family of shapes for high node congruence in free-form structures, Autom. Constr. 59 (2015) 38–47, http://dx.doi.org/10.1016/j.autcon.2015.07.009.

[40] Z. Shan, Q. Wang, H. Wu, B. Gao, Simplified quadrilateral grid generation of complex free-form gridshells by surface fitting, J. Build. Eng. 48 (2022) 103827, http://dx.doi.org/10.1016/j.jobe.2021.103827.

[41] C. Dunant, M. Drewniok, J. Orr, J. Allwood, Good early stage design decisions can halve embodied CO2 and lower structural frames' cost, Structures 33 (2021) 343–354, http://dx.doi.org/10.1016/j.istruc.2021.04.033.

[42] Q. Qiao, A. Yunusa-Kaltungo, R.E. Edwards, Towards developing a systematic knowledge trend for building energy consumption prediction, J. Build. Eng. 35 (2021) 101967, http://dx.doi.org/10.1016/j.jobe.2020.101967.

[43] S. Malek, The Effects of Geometry and Topology on the Mechanics of Gridshells (Ph.D. thesis), Massachussets Institute of Technology, 2012.

[44] C. Schittich (Ed.), Japanese Pavilion in Hanover: Architects: Shigeru Ban Architects, Birkhäuser, Tokyo, München, 2006, pp. 120–125.

[45] S. Colabella, B. D'Amico, E. Hoxha, C. Fivet, Structural design with reclaimed materials: an elastic gridshell out of skis, in: Proceedings of the IASS Annual Symposium 2017, Hamburg, Germany, 2017.

[46] J. Rombouts, G. Lombaert, L. De Laet, M. Schevenels, A novel shape optimization approach for strained gridshells: Design and construction of a simply supported gridshell, Eng. Struct. 192 (2019) 166–180, http://dx.doi.org/10.1016/j.engstruct.2019.04.101.

[47] W. Gythiel, M. Schevenels, Gradient-based size, shape, and topology optimization of single-layer reticulated shells subject to distributed loads, Struct. Multidiscip. Optim. 65 (2022) 144, http://dx.doi.org/10.1007/s00158-022-03225-w.

[48] V. Tomei, E. Grande, M. Imbimbo, Design optimization of gridshells equipped with pre-tensioned rods, J. Build. Eng. 52 (2022) 104407, http://dx.doi.org/10.1016/j.jobe.2022.104407.

[49] M. Konstantatou, W. Baker, T. Nugent, A. McRobie, Grid-shell design and analysis via reciprocal discrete Airy stress functions, Int. J. Space Struct. 37 (2022) 150–164, http://dx.doi.org/10.1177/09560599221081004.

[50] A. Favilli, F. Laccone, P. Cignoni, L. Malomo, D. Giorgi, Geometric deep learning for statics-aware grid shells, Comput. Struct. 292 (2024) 107238, http://dx.doi.org/10.1016/j.compstruc.2023.107238.

[51] Z. Li, B. Hu, G. Quan, B. Gao, Q. Wang, A structured grid generation framework based on parameterization for the design of free-form gridshells, J. Build. Eng. 62 (2022) 105400, http://dx.doi.org/10.1016/j.jobe.2022.105400.

[52] H. Lu, Y. Xie, Reducing the number of different members in truss layout optimization, Struct. Multidiscip. Optim. 66 (2023) 52, http://dx.doi.org/10.1007/s00158-023-03514-y.

[53] M. Kilian, D. Pellis, J. Wallner, H. Pottman, Material-minimizing forms and structures, ACM Trans. Graph. 36 (6) (2017) 1–12, http://dx.doi.org/10.1145/3130800.3130827.

[54] R. Mesnil, C. Douthe, O. Baverel, Non-standard patterns for gridshell structures: Fabrication and structural optimization, J. Int. Assoc. Shell Spatial Struct. 58 (2017) 277–286, http://dx.doi.org/10.20898/j.iass.2017.194.893.

[55] R. Mesnil, C. Douthe, C. Richter, O. Baverel, Fabrication-aware shape parametrisation for the structural optimisation of shell structures, Eng. Struct. 176 (2018) 569–584, http://dx.doi.org/10.1016/j.engstruct.2018.09.026.

[56] L. Bruno, P. Cignoni, S. Gabriele, E. Grande, M. Imbimbo, F. Laccone, F. Marmo, E. Mele, L. Raffaele, V. Tomei, F. Venuti, Freegrid:a benchmark on design and optimisation of free-edge gridshells, in: Proceedings of the IASS Annual Symposium 2023, Melbourne, 2023.

[57] L. Bruno, S. Gabriele, E. Grande, M. Imbimbo, F. Laccone, F. Marmo, E. Mele, L. Raffaele, V. Tomei, F. Venuti, Exploring new frontiers in gridshell design: The freegrid benchmark, Structures 58 (2023) 105678, http://dx.doi.org/10.1016/j.istruc.2023.105678.

[58] E. Vouga, M. Höbinger, J. Wallner, H. Pottman, Design of self-supporting surfaces, ACM Trans. Graph. 31 (4) (2012) 1–11, http://dx.doi.org/10.1145/2185520.2185583.

[59] L. Mourad, J. Bleyer, R. Mesnil, J. Nseir, K. Sab, W. Raphael, Topology optimization of load-bearing capacity, Struct. Multidiscip. Optim. 64 (3) (2021) 1367–1383, http://dx.doi.org/10.1007/s00158-021-02923-1.

[60] F. Taucer, E. Spacone, F. Filippou, A Fiber Beam–Column Element for Seismic Response Analysis of Reinforced Concrete Structures, Report, Earthquake Engineering Research Center College of Engineering University of California, Berkeley, 1991.

[61] R. Clough, K. Benuska, Nonlinear earthquake behavior of tall buildings, J. Eng. Mech. Div. 93 (1967) 129–146, http://dx.doi.org/10.1061/JMCEA3.0000855.

[62] M.K. Thompson, J.M. Thompson, ANSYS Mechanical APDL for Finite Element Analysis, Butterworth-Heinemann, 2017.

[63] ANSYS Mechanical APDL Release 22.2, Help System - ANSYS Inc., 2022.

[64] CSI Analysis Reference Manual - Computers and Structures Inc., 2021.

[65] A. Darby, T. Ibell, M. Evernden, Innovative use and characterization of polymers for timber-related construction, Materials 3 (2010) 1104–1124, http://dx.doi.org/10.3390/ma3021104.

[66] C. Haskell, N. Montagne, C. Douthe, O. Bavarel, C. Fivet, Generation of elastic geodesic gridshells with anisotropic cross sections, Int. J. Space Struct. 36 (4) (2021) 294–306, http://dx.doi.org/10.1177/09560599211064099.

[67] Structural Design Actions, Part 0: General Principles, Standard, Standards Australia, Sydney, 2002.

[68] J. Yan, F. Qin, Z. Cao, F. Fan, Y. Mo, Mechanism of coupled instability of single-layer reticulated domes, Eng. Struct. 114 (2016) 158–170, http://dx.doi.org/10.1016/j.engstruct.2016.02.005.

[69] V. Gioncu, N. Balut, Instability behaviour of single layer reticulated shells, Int. J. Space Struct. 7 (4) (1992) 243–252, http://dx.doi.org/10.1177/026635119200700402.

[70] R. Peek, Worst shapes of imperfections for space trusses with multiple global and local buckling modes, Int. J. Solids Struct. 30 (16) (1993) 2243–2260, http://dx.doi.org/10.1016/0020-7683(93)90085-L.

[71] F. Fan, J. Yan, Z. Cao, Stability of reticulated shells considering member buckling, J. Constr. Steel Res. 77 (2012) 32–42, http://dx.doi.org/10.1016/j.jcsr.2012.04.011.

[72] M. Mohammadi, K. Abedi, N. Taghizadieh, Stability analysis of single-layer barrel vault space structures, Int. J. Space Struct. 7 (4) (2012) 203–218, http://dx.doi.org/10.1260/0266-3511.27.4.203.

[73] H. Pottmann, Architectural geometry and fabrication-aware design, Nexus Netw. J. 15 (2013) 195–208, http://dx.doi.org/10.1007/s00004-013-0149-5.

[74] A.H. Bermano, T. Funkhouser, S. Rusinkiewicz, State of the art in methods and representations for fabrication-aware design, Comput. Graph. Forum 36 (2) (2017) 509–535, http://dx.doi.org/10.1111/cgf.13146.

[75] N. Pietroni, D. Tonelli, E. Puppo, M. Froli, R. Scopigno, P. Cignoni, Statics aware grid shells, Comput. Graph. Forum 34 (2) (2015) 627–641, http://dx.doi.org/10.1111/cgf.12590.

[76] C. Tang, X. Sun, A. Gomes, J. Wallner, H. Pottman, Form-finding with polyhedral meshes made simple, ACM Trans. Graph. 33 (4) (2014) 70:1–70:9, http://dx.doi.org/10.1145/2601097.2601213.

[77] Y. Eldar, M. Lindenbaum, M. Porat, Y. Zeevi, The farthest point strategy for progressive image sampling, IEEE Trans. Image Process. 6 (9) (1997) 1305–1315, http://dx.doi.org/10.1109/83.623193.

[78] A. Holgate, The Art of Structural Engineering: The Work of Jörg Schlaich and His Team, Edition Axel Menges, 1997.

[79] O. Gibbon, C. Archer-Jones, W. Arnold, D. Green, How to Calculate Embodied Carbon, second ed., London, 2022.

[80] R. Stroetmann, High strength steel for improvement of sustainability, in: Proceedings Eurosteel 2011, Budapest, Hungary, 2011.

[81] V. Tomei, M. Imbimbo, E. Mele, Optimization of structural patterns for tall buildings: the case of diagrid, Eng. Struct. 171 (2018) 280–297, http://dx.doi.org/10.1016/j.engstruct.2018.05.043.

[82] F. Cedron, A. Elghazouli, Assessment and design considerations for single layer cylindrical lattice shells subjected to seismic loading, Structures 31 (2019) 940–960, http://dx.doi.org/10.1016/j.istruc.2021.02.023.

[83] IASS WG8 for Metal Spatial Structures, Guide to Earthquake Response Evaluation of Metal Roof Spatial Structures, Tech. Rep., International Association for Shell and Spatial Structures, 2019.

[84] F. Rizzo, M. Barbato, V. Sepe, Peak factor statistics of wind effects for hyperbolic paraboloid roofs, Eng. Struct. 173 (2018) 313–330, http://dx.doi.org/10.1016/j.engstruct.2018.06.106.

[85] W. Liu, J. Ye, Collapse optimization for domes under earthquake using a genetic simulated annealing algorithm, J. Constr. Steel Res. 97 (2014) 59–68, http://dx.doi.org/10.1016/j.jcsr.2014.01.015.

[86] J. Ma, C. Wu, X. Zhi, F. Fan, Prediction of confined blast loading in single-layer lattice shells, Adv. Struct. Eng. 17 (7) (2014) 1029–1043, http://dx.doi.org/10.1260/1369-4332.17.7.1029.